
Article

Not peer-reviewed version

A New Methodology for Coastal Erosion Risk Assessment. Case Study: Calabria Region

[Giuseppina Chiara Barillà](#) ^{*} , [Giuseppe Barbaro](#) , [Giandomenico Foti](#) , Giuseppe Mauro

Posted Date: 6 November 2025

doi: 10.20944/preprints202511.0440.v1

Keywords: coastal erosion risk; index-based assessment; GIS integration; hazard; vulnerability; exposure



Preprints.org is a free multidisciplinary platform providing preprint service that is dedicated to making early versions of research outputs permanently available and citable. Preprints posted at Preprints.org appear in Web of Science, Crossref, Google Scholar, Scilit, Europe PMC.

Copyright: This open access article is published under a Creative Commons CC BY 4.0 license, which permit the free download, distribution, and reuse, provided that the author and preprint are cited in any reuse.

Disclaimer/Publisher's Note: The statements, opinions, and data contained in all publications are solely those of the individual author(s) and contributor(s) and not of MDPI and/or the editor(s). MDPI and/or the editor(s) disclaim responsibility for any injury to people or property resulting from any ideas, methods, instructions, or products referred to in the content.

Article

A New Methodology for Coastal Erosion Risk Assessment. Case Study: Calabria Region

Giuseppina Chiara Barillà ^{1,*}, Giuseppe Barbaro ¹, Giandomenico Foti ² and Giuseppe Mauro ¹

¹ Mediterranea University of Reggio Calabria (Italy), DICEAM Department, Via Graziella, loc. Feo di Vito, 89122 - Reggio Calabria, Italy

² Mediterranea University of Reggio Calabria (Italy), AGRARIA Department, loc. Feo di Vito, 89122 - Reggio Calabria, Italy

* Correspondence: chiara.barilla@unirc.it

Abstract

The coastal environment is a dynamic system shaped by both natural processes and human activities. In recent decades, increasing anthropogenic pressure and climate change—manifested through sea-level rise and more frequent extreme events—have accelerated coastal retreat, highlighting the need for improved management strategies and standardized tools for coastal risk assessment. Existing approaches remain highly heterogeneous, differing in structure, input data, and the range of factors considered. To address this gap, this study proposes an index-based methodology of general validity designed to quantify coastal erosion risk through the combined analysis of hazard, vulnerability, and exposure factors. The approach was developed for multi-scale and multi-risk applications and implemented across 54 representative sites along the Calabrian coast in southern Italy, demonstrating strong adaptability and robustness for regional-scale assessments. Results reveal marked spatial variability in coastal risk, with the Tyrrhenian sector exhibiting the highest values due to the combined effects of energetic wave conditions and intense anthropogenic pressure. The proposed framework can be easily integrated into open-access GIS platforms to support evidence-based planning and decision-making, offering practical value for public administrations and stakeholders, and providing a flexible, accessible tool for integrated coastal risk management.

Keywords: coastal erosion risk; index-based assessment; GIS integration; hazard; vulnerability; exposure

1. Introduction

Coastal areas host a significant proportion of the world's population and concentrate critical infrastructures, economic activities, and essential ecosystem resources [1,2]. Coastal erosion, together with sea-level rise, poses an increasing threat to these areas, with impacts ranging from the loss of emerged land and natural habitats to the degradation of ecosystem services, as well as direct damage to assets of outstanding natural, landscape, and historical–archaeological value, including settlements and strategic infrastructures [3–5]. At the global scale, the interaction between sea-level rise and anthropogenic pressures is undermining ecosystem services [6], producing critical effects in several contexts [7,8]. Consequently, coastal risk assessment today represents one of the most pressing scientific and operational challenges worldwide, within a framework characterized by increasing human pressure and the accelerating effects of climate change. In this context, there is an urgent need for reliable methodologies to assess risk and to support adaptation and sustainable management strategies.

Over the past decades, coastal risk assessment has evolved from purely physical approaches to integrated methodologies that jointly consider hazard, vulnerability, and exposure. The introduction of the Coastal Vulnerability Index (CVI) enabled comparative assessments of coastal vulnerability at

regional and national scales [9,10], but it also revealed limitations related to oversimplification and low adaptability to diverse geomorphological and socioeconomic contexts [11–14].

In Italy and across Europe, numerous studies have applied and adapted index-based methodologies—from the Regional Coastal Management Plan of Basilicata [15] to the Coastal Master Plan of Calabria [16], and risk assessments in Campania [17] and Molise [18]. Other examples include the validation of storm-impact frameworks in Emilia-Romagna [19], the application of the CVI in Apulia [20], and the development of specific indices for Mediterranean dune systems [21]. At a broader scale, relevant studies include assessments for the Northern Adriatic [22], the Portuguese coast [23], the French Mediterranean coastline [24], Scotland [25], and the UK physical-economic coastal vulnerability index [26].

At the international level, several recent studies have developed more advanced approaches, including GIS- and multicriteria-based analyses [27,28], AHP methods addressing uncertainty [29,30], multi-hazard indices [31,32], extreme-event assessments [33], and comparative analyses of empirical models [34]. Some works have integrated the CVI into planning and monitoring tools, as in the Gulf of Finland [35] and in Morocco, where Muzirafuti and Theocharidis [36] applied remote sensing and GIS to the Casablanca coastline. Other studies have combined numerical modelling and remote sensing to assess coastal erosion [37].

In parallel, new indices have been introduced to integrate geomorphological, climatic, and socioeconomic factors [38], such as the Italian ISMV [39] and the Integrated Coastal Vulnerability Index (ICVI) for Mexico [40], as well as multi-hazard approaches for European coastal cities [41]. GIS, remote sensing, and machine learning technologies have become central tools for ensuring accurate and scalable analyses [42–45]. At the same time, Nature-based Solutions (NbS) have demonstrated their effectiveness in mitigating erosion and flood risks [46–48]. Moreover, participatory and multiscale approaches have proven crucial to enhancing the robustness of assessments and supporting sustainable management policies [49,50].

Overall, the current state of the art shows a clear evolution toward increasingly complex, integrated, and adaptive methodologies that combine biophysical and socioeconomic indicators, GIS and remote sensing tools, probabilistic approaches, and nature-based solutions. However, as summarized in Table 1, which synthesizes most of the referenced methodologies, both national and international frameworks for coastal risk assessment remain characterized not only by diverse calculation methods depending on the coastal region under investigation [11,51], but also by a significant variety and dispersion of the factors on which these methods are based.

The analysis of Table 1 highlights that coastal risk assessments predominantly focus on morphological and hydrodynamic aspects—such as beach morphology, wave climate, coastal geology, and shoreline evolution trends—whereas factors related to anthropogenic pressures and terrestrial dynamics (e.g., riverine sediment supply, soil sealing, coastal and port structures, and precipitation) are less frequently considered. This imbalance underscores the persistent methodological heterogeneity and emphasizes the need to develop integrated and standardized approaches capable of systematically including the full range of variables influencing coastal risk. Consequently, there remains a strong demand for shared and replicable procedures that can reduce methodological discrepancies and enable consistent comparisons across different coastal areas.

Within this framework, the present study proposes an innovative approach aimed at filling this gap and strengthening resilient coastal management strategies. Recognizing that coastal erosion studies cannot be effectively addressed without a multidisciplinary and systemic perspective, the main objective of this research is to define a generalizable coastal risk assessment procedure that organically integrates all relevant factors. The proposed methodology, designed for the coasts of the Calabria region in southern Italy but extendable to the entire national territory, can be implemented within an open-source GIS platform and aims to provide an operational tool for public authorities, private entities, and stakeholders involved in coastal zone planning and management.

Table 1. Summary of the main referenced methodologies, encompassing national and international frameworks for coastal risk assessment, with indication of their application scale, study area, and the coastal hazard and vulnerability factors considered.

Publication	Application scale	Application area	SLR*	T*	WC*	R*	LST*	RST*	CG*	SET*	ECM*	SCM*	DS*	V*	CDS*	PS*	CSI*
Greco & Martino, 2014 [15]	Regional	Basilicata (Italy)			✓				✓	✓	✓	✓	✓	✓	✓	✓	
Barbaro, 2016 [16]	Regional	Calabria (Italy)			✓					✓	✓	✓			✓	✓	
Benassai et al., 2015 [17]	Sub-regional	Campania (Italy)	✓	✓	✓					✓	✓					✓	
Aucelli P. et al., 2017 [18]	Regional	Molise (Italy)			✓					✓	✓	✓	✓				
Armaroli & Duo, 2018 (CRAF) [19]	Regional	Emilia-Romagna (Italy)		✓	✓					✓	✓	✓					
Pantusa et al., 2018 [20]	Local	Apulia (Italy)	✓	✓	✓					✓	✓		✓	✓			
Ciccarelli et al., 2017 [21]	Regional	Tuscany & Sardinia (Italy)		✓	✓					✓	✓	✓	✓	✓			
Torresan et al., 2012 [22]	Regional	Friuli-Venezia Giulia (Italy)				✓	✓	✓					✓	✓	✓		
Ferreira Silva et al., 2017 [23]	Local	Portugal	✓	✓	✓					✓	✓	✓					
Mavromatidi et al., 2018 [24]	Regional	France	✓	✓	✓					✓	✓	✓					
Fitton et al., 2016 [25]	Local	Scotland			✓					✓		✓					
Kantamaneni et al., 2018 [26]	Local	United Kingdom										✓	✓	✓	✓	✓	
Satta et al., 2016 (MS-CRI) [12]	Local	Morocco	✓		✓	✓		✓	✓	✓		✓					
Satta et al., 2017 (CRI-MED) [13]	International	Mediterranean countries	✓		✓	✓				✓		✓					
Narra et al., 2017 (CERA) [14]	Local	Portugal & Mozambique		✓	✓				✓	✓	✓			✓		✓	
Mohamed, 2020 [27]	Sub-regional	Egypt	✓	✓	✓					✓	✓	✓	✓			✓	
Rehman et al., 2022 [28]	Local	India	✓	✓	✓					✓	✓	✓	✓				
Roy et al., 2021 [29]	Regional	Bangladesh	✓		✓					✓	✓	✓	✓				
Thirumurthy et al., 2022 [30]	Local	India	✓	✓		✓				✓	✓	✓					
Ariffin et al., 2023 [31]	Sub-national	Malaysia	✓							✓	✓	✓	✓			✓	
Barzehkar et al., 2024 [32]	National	Estonia	✓		✓					✓	✓	✓	✓			✓	
Ahmed et al., 2022 [33]	Local	India	✓	✓	✓					✓	✓						
Hossain et al., 2022 [34]	Sub-regional	India	✓	✓	✓					✓	✓	✓	✓				

Kovaleva et al., 2022 [35]	Regional	Russia	✓		✓	✓	✓
Muzirafuti & Theocharidis, 2025 [36]	Local	Morocco			✓	✓	✓
Nativí-Merchán et al., 2021 [37]	Local	Ecuador	✓	✓	✓	✓	✓
Godwyn-Paulson et al., 2022 [40]	Sub-national	Mexico	✓	✓	✓	✓	✓
Laino & Iglesias, 2024 [41]	Local	European coastal cities	✓	✓	✓		✓
Ennouali et al., 2023 [45]	Local	Morocco	✓	✓	✓	✓	✓
Mandal & Dey, 2022 [50]	Sub-national	India	✓	✓	✓	✓	✓

* SLR = Sea Level Rise; T = Tide; WC = Wave climate; R = Rainfall; LST = Longshore sediment transport; RST = River sediment transport; CG = Coastal geology; SET = Shoreline evolution trend; ECM = Emerged Coastal Morphology; SCM = Submerged Coastal Morphology; DS = Dune systems; V = Coastal vegetation; CDS = Presence of coastal defense structures; PS = Presence of Port structures; CSI = Degree of coastal surface impermeabilization.

2. Materials and Methods

2.1. Case Study: The Calabria Region

Calabria, located at the southernmost tip of the Italian peninsula, covers an area of approximately 15,079 km² and has a population of just over two million inhabitants. The region is divided into five provinces (Catanzaro, Cosenza, Crotone, Reggio Calabria, and Vibo Valentia) and includes 409 municipalities, 116 of which have coastal development. It borders Basilicata to the north, is bounded by the Tyrrhenian Sea to the west and the Ionian Sea to the east, and is separated from Sicily to the south by the Strait of Messina, which narrows to just 3.2 km at its closest point (Figure 1).



Figure 1. The Calabrian region (shown with red dotted line), in the center of the Mediterranean Sea.

The territory is predominantly hilly (49.2%) and mountainous (41.8%), with major mountain chains such as the Pollino, Catena Costiera, Sila, Serre, and Aspromonte ranges. The main lowland

areas are the plains of Sibari, Lamezia Terme, and Gioia Tauro. From a hydrographic perspective, Calabria is characterized by ephemeral and torrential watercourses known as fiumare, which are prone to sudden and intense floods, exhibit high sediment transport, and exert a strong influence on coastal dynamics. Numerous artificial lakes are also present, particularly on the Sila plateau.

The Calabrian coastline extends for approximately 736 km, alternating sandy and gravel beaches with stretches of high, rocky cliffs. Anthropogenic pressure is considerable, particularly around coastal provincial capitals and in areas with a strong touristic vocation, where recreational activities and beach facilities play a key role in the regional economy. The coastline can be subdivided into three main sectors: the Tyrrhenian (over 250 km), the Ionian (over 400 km), and the Strait of Messina (about 40 km). The Tyrrhenian and Ionian sectors are exposed to wave conditions associated with long fetches—sometimes exceeding 1,500 km—whereas the Strait of Messina is characterized by shorter fetches and a generally less energetic wave climate.

From a geomorphological standpoint, the Tyrrhenian coast is distinguished by a high proportion of steep cliffs (reaching up to 40% in some provinces), limited lowland areas, and a significant degree of urbanization along the remaining low-lying sectors. Conversely, the Ionian coast is dominated by alluvial plains that have historically favored human settlement, with approximately 30% of low-lying coasts occupied by anthropogenic activities. The coastal area of the Strait, finally, is densely urbanized due to both its narrow morphological configuration and its proximity to Sicily.

For this study, a total of 54 sampling sites were selected and distributed across the three coastal sectors of the region: 32 along the Ionian coast, 19 along the Tyrrhenian coast, and 3 within the Strait of Messina area, encompassing approximately 116 km of coastline (Figure 2). The selection of sites was guided by the availability of wave and meteorological data, as well as by the need to represent the diversity of coastal morphologies present along the study area. A list of the analyzed sites is provided in Table 2.

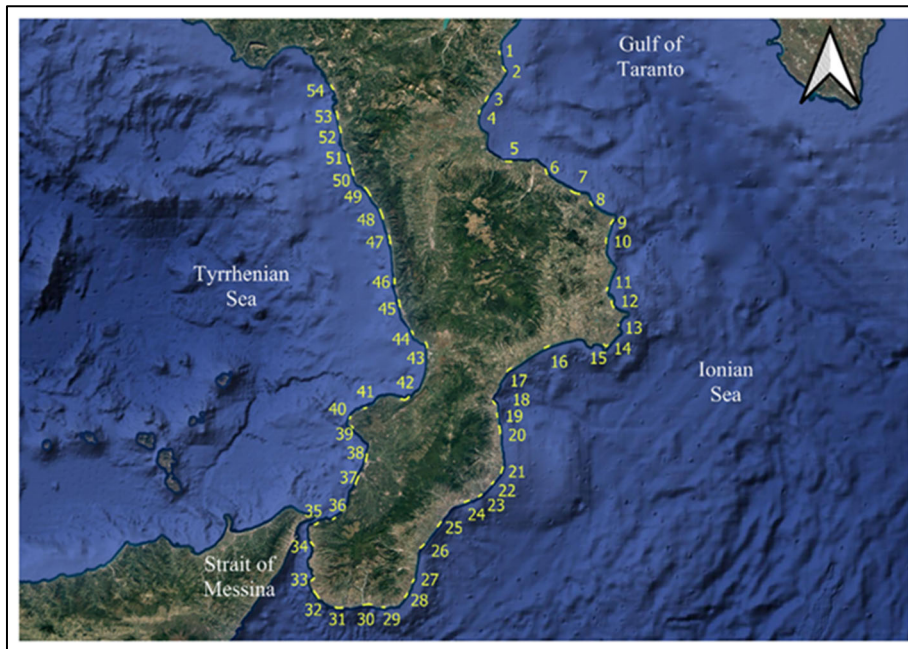


Figure 2. Location of the 54 sample sites in the Calabria region where the analysis was carried out: 1-32 along the Ionian coast, 33-35 within the Strait of Messina, 36-54 along the Tyrrhenian coast.

Table 2. List of the 54 sample areas in the Calabria region where the study was conducted: sites 1–32 are located along the Ionian coast, sites 33–35 within the Strait of Messina, and sites 36–54 along the Tyrrhenian coast.

N.	Sample area	N.	Sample area	N.	Sample area
1	Montegiordano	19	San Sostene	37	Palmi
2	Roseto Capo Spulico	20	Badolato	38	San Ferdinando
3	Trebisacce	21	Monasterace	39	Ricadi (Santa Maria)
4	Villapiana	22	Riace	40	Capo Vaticano
5	Rossano	23	Caulonia	41	Tropea
6	Calopezzati	24	Roccella Ionica	42	Vibo Marina
7	Cariati	25	Locri	43	Gizzeria
8	Crucoli (Torretta)	26	Bovalino	44	Falerna
9	Cirò Marina	27	Ferruzzano	45	Amantea
10	Torre Melissa	28	Brancaleone	46	Belmonte
11	Crotone (Zigari)	29	Palizzi	47	San Lucido
12	Crotone	30	Bova Marina	48	Fuscaldo
13	Isola Capo Rizzuto (Marinella)	31	Melito Porto Salvo	49	Cetraro
14	Isola Capo Rizzuto	32	Lazzaro	50	Sanginetto
15	Isola Capo Rizzuto (Le Castella)	33	Reggio Calabria (Pellaro)	51	Belvedere
16	Cropani	34	Reggio Calabria (Gallico)	52	Santa Maria del Cedro
17	Catanzaro Lido	35	Villa San Giovanni (Porticello)	53	Scalea
18	Soverato	36	Scilla (Favazzina)	54	Tortora

2.2. Methodological Framework

The methodology developed for coastal risk assessment is based on an index-based approach, selected for its ease of application and its potential integration within a GIS environment. Although calibrated for the Calabrian context, the method has general validity and can be adapted to different territorial scales (local, municipal, provincial, or interregional). The proposed model assesses the coastal risk index (I_R) as the product of three fundamental components:

$$I_R = I_H \cdot I_V \cdot I_E \quad (1)$$

where:

- Hazard Index (I_H): measures the intensity of natural forcing agents such as wave climate, wind, currents, and sea-level rise.
- Vulnerability Index (I_V): describes the susceptibility of the coastal system based on its geomorphological, ecological, and anthropogenic characteristics.
- Exposure Index (I_E): evaluates the assets and population located in areas potentially affected by coastal hazards.

Each index is computed as a weighted mean of its elementary variables, classified into five categories (1 = very low; 5 = very high) and subsequently normalized within the range 0–1. The normalization procedure follows the mathematical formulation proposed in the CRI-MED methodology [13]. Consequently, the hazard, vulnerability, and exposure indices are calculated using the following general expressions:

$$I_H = \frac{\sum_{i=1}^{n_h} h_i W_{h,i} - 1}{4} \quad (2)$$

$$I_V = \frac{\sum_{i=1}^{n_v} v_i W_{v,i} - 1}{4} \quad (3)$$

$$I_E = \frac{\sum_{i=1}^{n_e} e_i W_{e,i} - 1}{4} \quad (4)$$

where n_h , n_v and n_e represent the number of variables considered for hazard, vulnerability, and exposure, respectively; the weights W_h , W_v e W_e are assigned to each variable according to its relative contribution to the definition of hazard, vulnerability, and exposure in the context of coastal risk assessment.

Once estimated, the three indices (I_H , I_V , I_E) are classified according to the threshold values reported in Table 3.

Table 3. Classification of hazard, vulnerability and exposure indices.

Hazard/ Vulnerability/ Exposure Level	I_H / I_V / I_E
Low	< 20 %
Medium – low	20 ÷ 40 %
Medium	40 ÷ 60 %
Medium – high	60 ÷ 80 %
High	≥ 80 %

The developed methodology can be structured into five main phases, described in detail below (Figure 3):

1. Definition of the coastal hazard area;
2. Determination of the Coastal Hazard Indices and evaluation of the overall hazard index;
3. Determination of the Coastal Vulnerability Indices and evaluation of the overall vulnerability index;
4. Determination of the Coastal Exposure Indices and evaluation of the overall exposure index;
5. Evaluation of the final Coastal Risk Index.

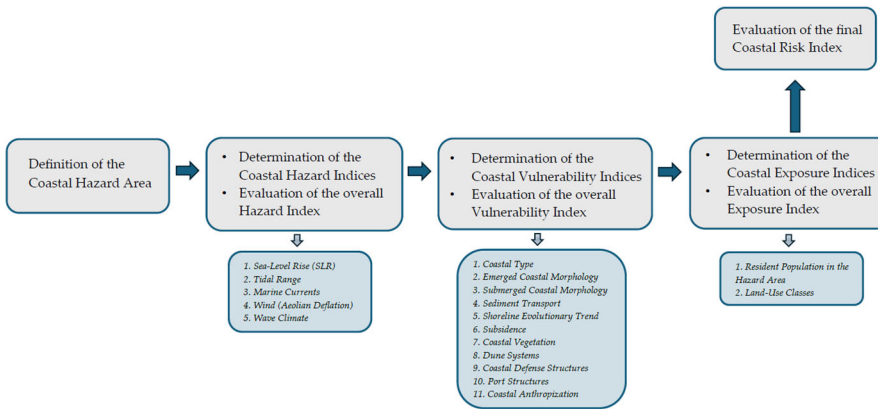


Figure 3. Flowchart of the new methodology developed for coastal risk assessment.

2.2.1. Definition of the Coastal Hazard Area

The coastal area potentially at risk is defined as the zone between the present shoreline and the maximum elevation reached by the sea level under extreme conditions. This elevation is determined as the sum of:

- Wave run-up and set-up (with a return period of 100 years);
- Astronomical and meteorological tides;
- Projected sea-level rise over a 100-year horizon according to the most severe IPCC scenario.

2.2.2. Hazard Indices

Coastal hazard factors are primarily related to the main climatic forcing agents that, with varying intensity and incidence, drive erosional processes. These include tides, currents, winds, waves, and, in particular, sea-level rise induced by global warming—an ongoing and unavoidable phenomenon in any contemporary coastal risk analysis.

Accordingly, the proposed model incorporates five main hazard sub-indices, accounting for the following components:

(1) *Sea-Level Rise (SLR)*. This sub-index is based on the rate of sea-level rise (mm/year), as estimated in numerous studies through satellite data analysis and assessments provided by the IPCC and NASA. Although SLR is a global-scale parameter with limited regional variability, it was considered essential to include it as a factor contributing to the long-term increase in hazard. As in many coastal vulnerability studies, this sub-index can be evaluated using the class intervals proposed by Pendleton et al. (2004) in their assessment of sea-level-rise-induced coastal vulnerability [52].

(2) *Tidal Range*. This parameter is based on the mean tidal range, measured in meters, derived from tide-gauge records. The corresponding index value is determined according to the five-class tidal regime classification proposed by Hayes (1979) [53].

(3) *Marine Currents*. This sub-index accounts for the influence of marine currents on coastal erosion, particularly in narrow straits or channels where geographic configuration enhances current velocity. Since increasing current velocity generally implies higher hazard, classes of hazard were defined as a function of the mean current speed (in knots). These values can be obtained from published datasets, tide tables, and nautical charts.

(4) *Wind (Aeolian Deflation)*. The wind-deflation index quantifies the direct effect of wind on coastal erosion, which is generally modest, and is a function of aeolian transport capacity. It is expressed as the percentage of annual hours during which wind velocity exceeds the critical threshold for sediment transport. This threshold, defined by Bagnold (1941) [54] based on sediment characteristics, can be estimated from wind data measured at 10 m above ground using the simplified relationship proposed by Hsu (1974) [55]. Comparing this critical velocity with observed wind time series allows the exceedance probability—and hence the site-specific index value—to be determined.

(5) *Wave Climate*. The wave-climate index (I_{WC}) was computed by dividing the Calabrian coastline into three macro-areas (Tyrrhenian, Strait of Messina, and Ionian) based on exposure and fetch. Following and refining the approach of Barbaro (2016), the updated formulation also accounts for secondary exposure sectors and wave run-up. The index is expressed as the weighted mean (equal weights) of four sub-indices ranging between 0 and 1, described below:

$$I_{WC} = 0.25 (I_{\phi} + I_{\alpha,\beta} + I_{\Delta h} + I_{Ru}) \quad (5)$$

where:

- I_{ϕ} is the wave energy flux index, defined as the ratio between the sum of the energy fluxes of the active (or incident) directional sectors at the site under examination and the maximum value recorded within the corresponding macro-area of reference.
- $I_{\alpha,\beta}$ is the index associated with the wave exposure sectors, defined as the weighted mean of the indices corresponding to the primary and, where applicable, the secondary wave-approach sectors, using their respective energy fluxes as weights. The primary sector corresponds to the direction of maximum wave energy, while the secondary sector refers to a secondary energy peak. The index for the primary sector accounts for the greater forcing exerted by waves approaching the shoreline orthogonally (shoaling) compared to more oblique waves (refraction), tending toward 1 as wave incidence becomes more perpendicular. The inclusion of the secondary sector allows the representation of conditions in which the coastline is influenced by multiple wave-attack directions, thereby extending the original formulation proposed by Barbaro (2016) [16].
- $I_{\Delta h}$ is the index related to the variation of significant wave height with return period, defined as the ratio between the mean value of $\Delta h(R)$ calculated for the different return periods at the site

under analysis and the corresponding maximum value computed for the reference macro-area. Here, $\Delta h(R)$ represents the difference in significant wave height calculated for successive return periods (1, 10, 20, 50, 100, 200, and 500 years).

- I_{Ru} is the index associated with the variation of wave run-up with return period, defined as the ratio between the mean value of $\Delta Ru(R)$ calculated for the different return periods at the site under analysis and the corresponding maximum value computed for the reference macro-area. Here, $\Delta Ru(R)$ represents the difference between the run-up values calculated for successive return periods at the same location. The run-up values were estimated using the empirical formulation proposed by Stockdon et al. (2006) [56].

The coastal hazard indices defined in the new methodology, together with their classification criteria, are reported in Table 4.

The overall Coastal Hazard Index (I_H) was defined as a weighted combination of five contributing factors: sea-level rise (20%), tidal range (10%), marine currents (10%), wind (10%), and wave climate (50%). The assignment of these weights was based on scientific evaluations specific to the Calabrian context and agreed upon in consultation with regional policy makers. In particular, the wave climate was identified as the dominant forcing agent driving coastal erosion processes, whereas tides, currents, and wind were considered to have a relatively minor influence. Sea-level rise, although currently less impactful, was included as a significant long-term factor due to its expected contribution to future coastal flooding and erosion.

A hazard classification can be established according to the value of the overall index, as summarized in Table 3.

Table 4. Definition of coastal hazard indices according to the new methodology, including corresponding weights and the adopted classification criteria.

INDEX	W_h	Hazard Classes				
		Very low 1	Low 2	Moderate 3	High 4	Very high 5
SLR [mm/year]	0.2	< 1.8	1.8 ÷ 2.5	2.5 ÷ 3.0	3.0 ÷ 3.4	≥ 3.4
Tidal range [m]	0.1	< 1	1 ÷ 2	2 ÷ 3.5	3.5 ÷ 5	≥ 5
Marine Currents [knots]	0.1	< 0.5	0.5 ÷ 1.5	1.5 ÷ 3	3 ÷ 5	≥ 5
Wind (Aeolian Deflation) [%]	0.1	< 5	5 ÷ 15	15 ÷ 25	25 ÷ 35	≥ 35
Wave Climate	0.5	< 0.2	0.2 ÷ 0.4	0.4 ÷ 0.6	0.6 ÷ 0.8	≥ 0.8

2.2.3. Coastal Vulnerability Indices

Coastal vulnerability factors represent the elements through which the susceptibility of a coastal system to erosional processes can be assessed. They derive from a combination of natural and anthropogenic characteristics that jointly determine shoreline stability. In particular, geological and geomorphological conditions—both in the emerged and submerged zones—play a central role, as does the analysis of historical shoreline evolution, which helps to identify erosional or accretional trends.

Equally important is the balance between littoral drift and fluvial sediment inputs, which directly affects sediment availability along the coast. Additional factors include the presence of coastal defense structures and port infrastructures, as well as dune systems and vegetation cover, which can either exacerbate or mitigate erosional processes. Finally, parameters such as subsidence rates and the degree of soil sealing further contribute to defining the overall level of coastal vulnerability.

Accordingly, the proposed methodology considers eleven coastal vulnerability variables, grouped as follows:

(1) *Coastal Type*. Based on the most widely adopted morphological classification, which distinguishes between high rocky coasts and low sandy coasts, the vulnerability classes for this index

were defined using the scheme proposed by Ferreira et al. (2017) [57], considered particularly suitable for representing the conditions of the Calabrian coastal environment.

(2) *Emerged Coastal Morphology*. The vulnerability of the emerged coast was assessed as a function of two parameters: beach slope and mean beach width. Gently sloping and narrow beaches are more exposed to erosional and flooding processes than wider and steeper ones. Both parameters were estimated using transects derived from satellite imagery and Digital Terrain Models (DTMs) (Google Earth, QGIS). Vulnerability classes were defined by adapting the classification of Ferreira et al. (2017) [57] to the Calabrian context. The overall index was calculated as the arithmetic mean of the two sub-indices, with equal weighting.

(3) *Submerged Coastal Morphology*. The vulnerability of the submerged coast was evaluated based on seafloor slope, since steeper profiles lead to increased wave run-up and, consequently, greater exposure to erosion. This parameter can be estimated through the analysis of available bathymetric data, while vulnerability classes were defined by adapting the scheme of Ferreira et al. (2017) [57] to the geomorphological characteristics of the Calabrian coast.

(4) *Sediment Transport*. Coastal vulnerability is strongly influenced by the sediment budget, expressed as the ratio between fluvial sediment supply and longshore sediment transport, the latter being controlled by meteorological–marine forcing and sediment grain-size characteristics. In this study, the balance was expressed by an index defined as the ratio between Q_r and Q_l , where Q_r represents the fluvial sediment input to the physiographic unit and Q_l the longshore sediment transport. Index values greater than or equal to 1 indicate low vulnerability conditions, while values tending to zero correspond to critical sediment deficit conditions and thus to high vulnerability. The estimation of sediment transport rates can be performed through a simplified modelling approach, which, although less detailed than full numerical modelling, provides a reliable order-of-magnitude assessment suitable for comparing the two contributions and classifying vulnerability.

(5) *Shoreline Evolutionary Trend*. The shoreline evolution trend was evaluated following the methodology of Foti et al. (2022) [58], based on the comparison of cartographic datasets and satellite imagery. The overall index was computed as a weighted mean of the shoreline-change rates for different time intervals, assigning greater weight to the most recent data, which are more representative of current vulnerability conditions and characterized by higher positional accuracy. The vulnerability classes were defined according to the classification proposed by Barbaro (2016) [16].

(6) *Subsidence*. Subsidence, often of anthropogenic origin, constitutes a significant factor of coastal vulnerability as it amplifies the effects of storm surges and sea-level rise. In this study, the vulnerability classes, expressed as a function of the mean subsidence rate (mm/year), were calibrated based on available studies for the Calabrian areas affected by this phenomenon.

(7) *Coastal Vegetation*. Coastal vegetation represents a key element for shoreline resilience and morphological stability, as it contributes to the dissipation of wave energy and consequently to the reduction of erosional processes during extreme events [59–61]. Marine vegetation plays an equally relevant role: in particular, *Posidonia oceanica* constitutes a critical factor in mitigating coastal erosion and preserving sandy beaches, while maintaining benthic biodiversity—highlighting its importance as a natural defense mechanism for coastal systems [62–64]. Accordingly, a vegetation vulnerability index was defined as the weighted mean of three sub-indices: average width of coastal vegetation, corrected for vegetation density (with weight equal to 40%); percentage of coastline protected by vegetation (with weight equal to 40%); presence/absence of *Posidonia oceanica* (with weight equal to 20%). Vulnerability classes were defined by adapting the schemes proposed by Sekovski et al. (2020) [65] and Pantusa et al. (2018) [20] to the Calabrian context. The three sub-indices were evaluated using satellite data (Google Earth, QGIS) and historical datasets containing information on the mapping of coastal habitats.

(8) *Dune Systems*. Coastal dune systems act as natural defenses against erosion and flooding, functioning as sediment reservoirs, physical barriers, and hydrogeological buffers against saltwater intrusion [66,67]. Their development—strongly influenced by waves, wind, sediment supply, and psammophilous vegetation—is characterized by a zonation of plant cover that promotes dune

formation and stabilization. However, dune systems are highly vulnerable to climate change and anthropogenic pressures, which have progressively reduced their extent and protective capacity [68]. Given their role in enhancing coastal resilience, a dune-system vulnerability index was defined as the weighted mean of three sub-indices: average dune elevation (with weight equal to 30%), average dune width (with weight equal to 30%), percentage of coastline protected by dunes (with weight equal to 40%). Vulnerability classes were adapted from Sekovski et al. (2020) [65] and Pantusa et al. (2018) [20] to fit the Calabrian coastal conditions. The analysis was performed using satellite imagery, Digital Terrain Models (DTMs), and GIS tools (Google Earth, QGIS).

(9) *Coastal Defense Structures.* The presence of coastal defense structures significantly influences shoreline vulnerability, as these interventions alter littoral currents and sediment transport processes, and in some cases may exacerbate local erosion. The coastal defense index was therefore defined as the ratio between the length of protected shoreline (PSL) and the total coastline length, corrected to account for the state of preservation of the defense structures. The assessment was performed through satellite imagery and GIS-based analysis (Google Earth). With regard to the determination of PSL, which varies depending on the type of structure, this study provides the following methodological approach:

- if the structure is an emerged barrier, the PSL is assumed to be equal to the length of the barrier itself;
- if the structure is a submerged barrier, the PSL is estimated as the length of the barrier multiplied by a coefficient corresponding to the wave transmission coefficient of the structure, calculated in this study using the empirical formulation proposed by Van der Meer (1990) [69].
- If the structure in question is a groyne, the corresponding PSL is evaluated based on both its length and the angle of incidence of the predominant wave direction.
- In the case of a T-head groyne, that is a combination of a groyne and a breakwater, the PSL is calculated as the sum of the contributions attributed to the breakwater and the groyne components.

The highest vulnerability values occur along coastal stretches already affected by erosion but poorly protected, whereas unprotected shorelines without coastal defense structures are assigned a null score.

(10) *Port Structures.* Port infrastructures can significantly alter littoral dynamics by interrupting or reducing sediment transport, often triggering localized erosional processes. The corresponding port-structure vulnerability index was defined as a function of the maximum cross-shore extension of the port basin (A), normalized with respect to the maximum regional value. In the absence of port facilities, the index assumes a null value.

(11) *Coastal Anthropization.* The coastal anthropization vulnerability index was defined as the percentage of shoreline that has been artificially modified or hardened (i.e., non-erodible coastal segments). As the proportion of urbanized or engineered coastline increases, the vulnerability to erosion decreases, since the shoreline no longer coincides with the natural beach-sea interface but with built structures or infrastructures protected by revetments or seawalls.

The coastal vulnerability indices defined in the proposed methodology, along with their respective classification criteria, are summarized in Table 5.

The overall Coastal Vulnerability Index (I_V) was defined as the mean value of eleven sub-indices, corresponding to the following factors: coastal type, emerged and submerged morphology, sediment budget, shoreline evolution, subsidence, vegetation, dune systems, coastal defense structures, port infrastructures, and degree of anthropization. Each sub-index was assigned an equal weight (1/11), as the relative importance of the individual factors had already been accounted for in the definition of their respective vulnerability classes. A classification of vulnerability levels can be established according to the value of the overall index, as summarized in Table 3.

Table 5. Definition of vulnerability indices according to the new methodology, including corresponding weights and the adopted classification criteria.

INDEX	W_v	Vulnerability Classes				
		Very low 1	Low 2	Moderat e 3	High 4	Very high 5
Coastal type	1/11	High rocky coasts	Medium cliffs, irregular coasts	Low cliffs, alluvial plains	Sandy beaches, estuaries, lagoons	Sandy beaches, dune systems
Emerged Coastal Morphology (ECM)	Beach slope [%] ($w = 0.5$)	≥ 12	$12 \div 9$	$9 \div 6$	$6 \div 3$	< 3
	Mean beach width [m] ($w = 0.5$)	1/11	≥ 80	$80 \div 60$	$60 \div 40$	$40 \div 20$
Submerged Coastal Morphology – Seafloor slope [%]	1/11	< 2	$2 \div 6$	$6 \div 10$	$10 \div 20$	≥ 20
Sediment Transport (ST)	1/11	≥ 1	$1 \div 0.75$	$0.75 \div 0.5$	$0.5 \div 0.25$	< 0.25
Shoreline Evolutionary Trend (SET) [m/year]	1/11	≥ 0.5	$0.5 \div -0.5$	$-0.5 \div -1.0$	$-1.0 \div -2.0$	< -2.0
Subsidence (S) [mm/year]	1/11	≥ -1	$-1 \div -4$	$-4 \div -7$	$-7 \div -10$	< -10
Vegetation (V)	Average vegetation width [m] ($w = 0.4$)	≥ 100	$75 \div 100$	$50 \div 75$	$25 \div 50$	< 25
	Percentage of vegetative coverage [%] ($w = 0.4$)	1/11	≥ 80	$80 \div 60$	$60 \div 40$	$40 \div 20$
	Posidonia Oceanica ($w = 0.2$)			Presence (0) / Absence (5)		
Dune Systems (DS)	Average dune elevation [m] ($w = 0.3$)	≥ 6	$4 \div 6$	$2 \div 4$	$1 \div 2$	< 1
	Average dune width [m] ($w = 0.3$)	1/11	≥ 100	$75 \div 100$	$50 \div 75$	$25 \div 50$
	Percentage of coastline protected by dunes [%] ($w = 0.4$)		≥ 80	$80 \div 60$	$60 \div 40$	$40 \div 20$
Coastal Defense Structures (CDS) [%]	1/11	≥ 80	$80 \div 60$	$60 \div 40$	$40 \div 20$	< 20
Port Structures (PS)	1/11	< 0.2	$0.2 \div 0.4$	$0.4 \div 0.6$	$0.6 \div 0.8$	≥ 0.8
Coastal Anthropization (CA) [%]	1/11	≥ 80	$80 \div 60$	$60 \div 40$	$40 \div 20$	< 20

2.2.4. Coastal Exposure Indices

The assessment of elements exposed to coastal risk was carried out by considering two main indices: resident population within the hazard area and land-use classes. Although this approach does not provide a detailed socio-economic valuation, it is based on legislative and regulatory

references and allows for an effective differentiation and reliable representation of the value of exposed assets along eroding coastal sectors.

(1) *Resident Population within the Hazard Area*. The population exposure index was estimated following the methodology of the EUROSION Project (2004) [70], using ISTAT (2020) demographic data [71] and CORINE Land Cover (CLC 2018) shapefiles [72]. Population counts were calculated as the sum of residents within urban, agricultural, and natural areas, weighted according to their respective population densities. The exposure index increases proportionally with the number of residents located within the hazard zones.

(2) *Land-Use Classes*. The land-use exposure index was developed in compliance with current risk-assessment regulations, using CLC 2018 shapefiles and cartographic data from the Regional Geoportal [73]. The classification of exposed elements was based on the categories of potential damage indicated in the Operational Guidelines for the Implementation of Directive 2007/60/EC [74], in order to represent the socio-economic value associated with different land-use types. The level of exposure increases proportionally with the relevance of the category, in relation to the potential impact on people, economic assets, environmental resources, and cultural heritage. The overall land-use exposure index was calculated as the mean of three sub-indices, corresponding to areal, linear, and point-type shapefiles, thereby integrating all available spatial information in a consistent way.

The exposure indices defined in the proposed methodology, along with their respective classification criteria, are summarized in Table 6.

Based on scientific evaluation and consultation with regional policy makers, a weight of 20% was assigned to the population exposure index and 80% to the land-use exposure index, since the latter represents a broader and more diverse set of exposed elements.

Once calculated, the overall Coastal Exposure Index (I_E) can be classified according to the threshold values reported in Table 3.

Table 6. Definition of exposure indices according to the new methodology, including corresponding weights and the adopted classification criteria.

INDEX	W_e	Exposure Classes				
		Very low 1	Low 2	Moderate 3	High 4	Very high 5
Resident population in the hazard area [inhabitants]	0.2	< 1000	1000 ÷ 5000	5000 ÷ 10000	10000 ÷ 20000	≥ 20000
Land-Use Classes	0.8	Inland and coastal wetlands, Continental and marine waters, Bare rocks, cliffs, and rocky outcrops	Wooded areas, Natural grasslands and pastures, Sparsely vegetated areas, Transitional woodland-shrub	Arable land, Permanent crops (vineyards, olive groves, orchards, etc.), Sclerophyllous vegetation areas, Beaches, dunes, and sands	Extractive areas, Landfills, Cemeteries, Geosites	Residential urban areas, Industrial, commercial, and infrastructural areas, Construction sites, Urban green areas, Recreational and sports areas, Historical monuments and/or archaeological sites, Oases and nature reserves, National and Regional Parks, SACs, SINs, SIRs

2.2.5. Coastal Risk Index

Finally, the coastal risk index (I_R) is estimated using Equation (1). Accordingly, for each analyzed site, and based on the value of the final index, the coastal risk level is evaluated following the classification proposed in the Italian application of the EUROSION Project [70,75]. This classification is expressed on a percentage scale and summarized in Table 7.

Table 7. Classification of the Coastal Risk Index.

Risk Level	I_R
Low	< 5%
Medium - low	5 ÷ 15 %
Medium	15 ÷ 30 %
Medium – high	30 ÷ 50 %
High	≥ 50 %

3. Results

The proposed coastal erosion risk assessment methodology was applied to 54 sample sites distributed along the three main coastal sectors of Calabria. The analysis integrated geomorphological, meteomarine, hydrological, and anthropogenic data, enabling a comprehensive characterization of coastal hazard, vulnerability, exposure, and overall risk conditions. Table 8 summarizes the data and their corresponding sources used for the estimation of the variables involved in the developed methodology.

Table 8. Data used and their sources.

Data	Data source	Period
SLR (mm/year)	Literature studies [76]	1993-2023
SLR projections (mm/year)	Sea Level Projection Tool [103]	-
Hydrometric level data (m)	Tide gauge records – RMN (ISPRA) [78]	2010-2021
Current velocity (knots)	Literature studies [80,81]	-
Wind data (wind speed and direction)	MeteOcean Group – DICCA, University of Genoa [77]	1979-2018
Wave data (Hs, Tp, Tm, Dir)	MeteOcean Group – DICCA, University of Genoa [77]	1979-2018
Temperature data	Calabria Multi-Risk Functional Center [100]	1916–present
Rainfall data	Calabria Multi-Risk Functional Center [100]	1916–present
Coastline orientation	Satellite Imagery (Google Earth)	2021
Subsidence (mm/year)	Literature studies [88–97]	-
Beach slope (%)	Satellite Imagery (Google Earth)	2021
Beach width (m)	Satellite Imagery (Google Earth)	2021
Dn50 (mm)	OKEANOS (2003) [83]	2003
Foreshore beach slope (m)	EMODnet Digital Bathymetry (DTM 2020) [84]	2020
	Satellite Imagery (Google Earth)	2015-2021
Shoreline change rate (m/year)	Historical shorelines – Calabrian Geoportal [73] Orthophotos – Italian Geoportal [85]	1954; 1998; 2000; 2008 1989; 1996; 2006; 2012
Elevation	DTM 5x5 m – Calabrian Geoportal [73]	2008
Land use and land cover data (LULC data)	Level IV Corine Land Cover (2018) dataset [72]	2018
Posidonia Oceanica	MEDISEH Project [86]	2013
Coastal vegetation characteristics	Satellite Imagery (Google Earth)	2021
Dunal system characteristics	Satellite Imagery (Google Earth)	2021
Coastal Defense Structures and Ports	Satellite Imagery (Google Earth)	2021

Coastal Anthropization Population	Satellite Imagery (Google Earth) ISTAT Dataset [71]	2021 2020
--------------------------------------	--	--------------

3.1. Coastal Hazard

The analysis of the hazard variables considered allowed the evaluation of sea-level rise (SLR) for all study areas, adopting a growth trend of 4.5 mm/year, consistent with satellite-based studies [76]. Consequently, the corresponding hazard index was classified in the fifth class (very high hazard level) for all the examined sites, since SLR estimates are derived from global-scale datasets whose variation is not significant at regional scale.

For the wind data analysis, provided by the MeteOcean Group for the period 1979–2018 [77], 52 grid points distributed along the three Calabrian coastal sectors were considered. The 10 m wind-speed time series were processed to derive prevailing wind directions and intensities, with data grouped into 10° directional sectors and 1 m/s speed classes. From these analyses, both the maximum wind set-up and the exceedance probability of the critical wind velocity required to initiate aeolian sediment transport were estimated, the latter being adopted as a representative index of the process.

The calculated wind set-up values for the 54 sampled sites ranged between 0.6 and 17 cm. For aeolian transport computations, the critical wind velocity values ($u_{*,10m}$) ranged between 10 and 84 m/s. A detectable sediment transport capacity was identified in 20 out of the 54 sites, with the highest exceedance probability (6.9%) recorded at Brancaleone Marina, where the prevailing wind direction was from the southwest (SW) and the maximum observed wind speed reached 28 m/s. Regarding the wind-related hazard index, all sites were classified in the first class (very low hazard), except for Ferruzzano and Brancaleone, where the percentage of annual hours with active aeolian sediment transport ranged between 5% and 15%.

The mean tidal range was estimated using tide-gauge data from the National Tide Gauge Network (ISPRA) [78] for the period 2010–2021. Since only two stations are operational in Calabria (Reggio Calabria and Crotone), the analysis was extended to nearby stations—Catania, Taranto, and Palinuro—to ensure more comprehensive spatial coverage. The data, after removing outliers, were analyzed on an annual basis to determine the mean minimum and maximum sea levels and thus the mean tidal range, which was then assigned to the different Calabrian coastal sectors according to their proximity to the respective reference stations. The analysis yielded mean tidal range values of 0.87 m at Taranto, 0.90 m at Crotone, 0.72 m at Catania, 0.69 m at Reggio Calabria, and 0.88 m at Palinuro. These measurements were then spatially interpolated to assign representative values to the different coastal sectors of Calabria. Specifically, the Taranto value was adopted for the Upper Ionian coast within the Gulf of Taranto, while the Crotone value was applied to most of the Central Ionian sector. The Catania and Reggio Calabria data were considered representative of the Lower Ionian coast and the Strait of Messina, respectively, whereas the Palinuro value was used for the entire Tyrrhenian coastline. All sites therefore exhibit mean tidal ranges on the order of centimeters and below one meter, corresponding to a microtidal regime, consistent with Sannino et al. (2015) [79]. Consequently, despite minor spatial variations, all the examined locations were classified within the first hazard class for the tidal-range parameter.

In Calabria, marine currents are generally weak, ranging between 0.4 and 0.7 knots, but within the Strait of Messina they reach exceptional values, with mean intensities of 1–2 m/s and peaks up to 5 m/s [80]. The hydrodynamics of the area are dominated by semi-diurnal tidal currents, supplemented by drift and gradient currents as well as local circulation phenomena (countercurrents and vortices), which make this area unique within the Mediterranean and of particular interest for potential marine energy applications [81]. The marine current index exhibits values ranging between 1 and 4, reaching its maximum at Porticello, located in the southernmost sector of the Strait of Messina.

The wave climate off the Calabrian coasts was reconstructed using data provided by the MeteOcean Group (1979–2018) [77], integrated with simulations from the ABRCMaCRO software for the Strait of Messina. The region was divided into three macro-areas—Tyrrhenian, Ionian, and

Strait—based on exposure and fetch characteristics. A total of 51 grid points were analyzed (32 along the Ionian coast and 19 along the Tyrrhenian coast), while in the Strait of Messina, model data were replaced owing to inadequate spatial resolution. In the Tyrrhenian Sea, wave directions are concentrated within a few dominant sectors, primarily from the western quadrants (250° – 310°), with almost no secondary exposure sectors. Conversely, the Ionian coast is exposed to a much broader range of wave directions, predominantly from the southeast (100° – 140°), but with several secondary approach sectors that increase both variability and hazard—particularly along the Crotone shoreline, which also exhibits the highest wave energy fluxes (>7000 N/s). The higher hazard levels observed along the Ionian coasts are also supported by the wave statistical parameters, which indicate a more pronounced increase in significant wave heights with return period compared to the Tyrrhenian sectors. The wave run-up values, on the other hand, are strongly influenced by seabed slope, to a greater extent than by wave climate itself; consequently, the highest run-up values are recorded along the steep coasts of the Strait of Messina. In summary, the Calabrian wave climate exhibits substantial spatial variability: it is more concentrated and energetic along the Tyrrhenian coast, and more complex and potentially hazardous along the Ionian coast, with direct implications for shoreline vulnerability [82]. The wave-climate hazard index estimated for the analyzed sites ranged from moderate (third class) to very high (fifth class), with the highest scores found in the Strait of Messina and Tyrrhenian localities.

Table 9 reports the normalized overall hazard index values obtained for each analyzed site, computed using Equation (2) and weighted according to the coefficients provided in Table 4, together with their corresponding hazard classification. The results indicate medium-to-high hazard levels across all Tyrrhenian sites and variable levels, from medium to medium-high, along the Ionian coast and within the Strait of Messina (Figure 4).

Table 9. Normalized values of the overall coastal hazard index calculated for each analyzed site according to the proposed methodology.

N.	I_H	Hazard level	N.	I_H	Hazard level	N.	I_H	Hazard level
1	0.45	Medium	19	0.48	Medium	37	0.73	Medium – high
2	0.45	Medium	20	0.60	Medium – high	38	0.60	Medium – high
3	0.45	Medium	21	0.60	Medium – high	39	0.60	Medium – high
4	0.45	Medium	22	0.60	Medium – high	40	0.73	Medium – high
5	0.45	Medium	23	0.60	Medium – high	41	0.73	Medium – high
6	0.45	Medium	24	0.60	Medium – high	42	0.60	Medium – high
7	0.45	Medium	25	0.60	Medium – high	43	0.60	Medium – high
8	0.45	Medium	26	0.60	Medium – high	44	0.73	Medium – high
9	0.58	Medium	27	0.63	Medium – high	45	0.73	Medium – high
10	0.58	Medium	28	0.63	Medium – high	46	0.73	Medium – high
11	0.58	Medium	29	0.48	Medium	47	0.73	Medium – high
12	0.45	Medium	30	0.48	Medium	48	0.73	Medium – high
13	0.58	Medium	31	0.48	Medium	49	0.73	Medium – high
14	0.58	Medium	32	0.48	Medium	50	0.73	Medium – high
15	0.48	Medium	33	0.48	Medium	51	0.73	Medium – high
16	0.60	Medium – high	34	0.50	Medium	52	0.73	Medium – high
17	0.60	Medium – high	35	0.78	Medium – high	53	0.73	Medium – high
18	0.48	Medium	36	0.60	Medium – high	54	0.60	Medium – high

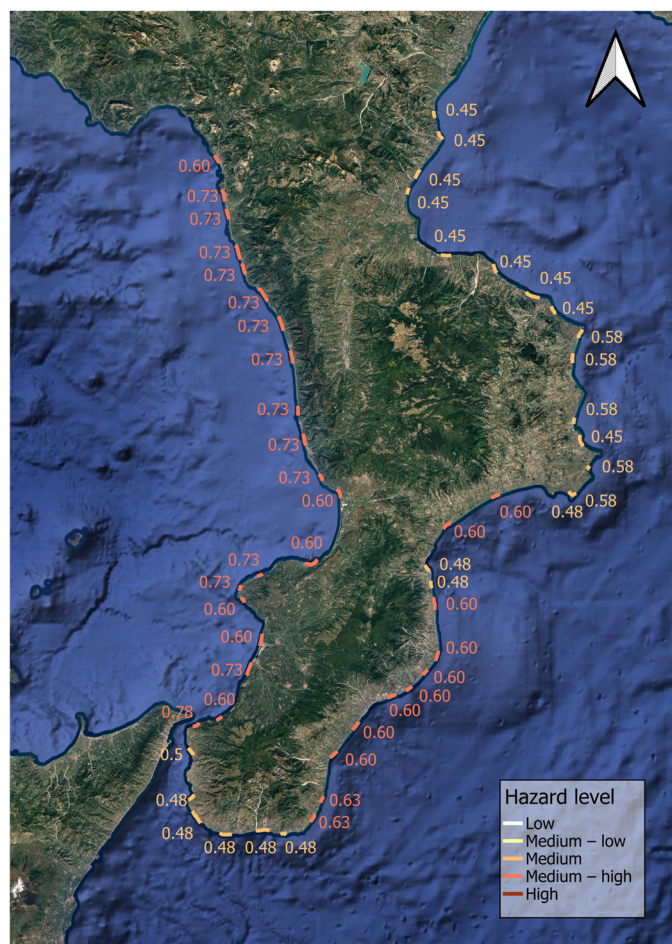


Figure 4. Hazard map.

3.2. Coastal Vulnerability

Regarding the vulnerability variables analyzed, all the selected sample sites consist of sandy beaches and therefore fall within the fifth (highest) vulnerability class for the coastal type index.

The Emerged Coastal Morphology Index (ECM) values range between 2.5 and 5, with the highest value recorded at Calopezzati. Sedimentological analysis based on OKEANOS (2003) data [83] highlights marked variability among the three macro-areas. Along the Ionian coast, emerged beaches are mainly composed of pebbles, gravel, and coarse sand, whereas seabed sediments show greater heterogeneity, ranging from coarse to fine materials (Dn_{50} up to 0.1 mm). In the Strait of Messina, emerged beaches are dominated by very coarse sands and pebbles, while the seabed consists of fine sands (0.13–0.18 mm). Along the Tyrrhenian coast, emerged sediments are predominantly gravelly and coarse, gradually transitioning to medium and fine sands at greater depths (up to 0.05 mm in the central Tyrrhenian sector). Morphological analysis of the emerged beach, based on satellite imagery (QGIS, Google Earth), revealed widths between 13 and over 100 m and slopes ranging from 2% to 17%. Coastal plains with wider lowlands are associated with broader, gentler beaches, while narrower plains typically correspond to steeper and narrower beaches.

For the Submerged Coastal Morphology Index (SCM), representing seabed slope, most sites fall into the first or second vulnerability classes, except for Rossano (Ionian coast) and the Strait of Messina, which show steeper profiles. Bathymetric analysis based on EMODnet-Bathymetry data [84] revealed average seabed slopes of 2–3% for both Tyrrhenian and Ionian sectors, with the exception of Rossano (10%), while the Strait of Messina exhibits much higher values, exceeding 20%, consistent with its unique geomorphological setting.

The Shoreline Evolutionary Trend Index (SET) spans all vulnerability classes: 13 sites show shoreline advancement (class 1), 28 sites are stable (class 2), 6 sites experience mild erosion (class 3),

6 sites show intense erosion (class 4), and one site experiences severe erosion (class 5). The shoreline evolution of Calabria was reconstructed through comparison of historical shorelines, orthophotos, and satellite imagery [73,85], analyzing over 700 transects and computing the Net Shoreline Movement (NSM) and End Point Rate (EPR) indices. Results indicate overall long-term stability, although significant local erosion issues persist. The highest recent erosion rate was recorded at Marina di Caulonia (\approx 6 m/year), followed by Calopezzati, San Ferdinando, and Belmonte Marina (\approx 3 m/year). Short-term analyses reveal strong erosion at Gizzeria Lido (5.5 m/year) and Crotone-Zigari (3.6 m/year). Shoreline advancement is generally limited (<1 m/year), except at Badolato, where harbor construction altered local sediment dynamics. Overall, Calabria's coastline exhibits widespread stability, though with vulnerable segments affected by anthropogenic pressures and local morphodynamic conditions [58].

The Dune System (DS) and Vegetation (V) indices vary between 1.9–5 and 2.4–5, respectively. The highest values correspond to areas where these natural protective systems are absent, resulting in maximum vulnerability. Dune and vegetation analyses conducted using QGIS and satellite imagery identified dunes up to 7 m in height and 94 m in width (Monasterace, Badolato) and vegetation widths up to 86 m (Badolato) or 80% coverage (Isola di Capo Rizzuto). Approximately 30 Posidonia oceanica meadows were mapped, mainly along the Ionian coast and within protected areas (Isola Capo Rizzuto, Costa degli Dei, Upper Tyrrhenian), based on information processed within the Mediterranean Sensitive Habitats (MEDISEH) project [86], underscoring their ecological importance and the better conservation state of less urbanized coasts. Anthropogenic pressure has drastically reduced Calabrian dune systems, intensifying coastal erosion along the Tyrrhenian coast. Urbanization in areas like Tortora has caused shoreline retreat, while partially preserved dunes in Villapiana have favored progradation [87].

Subsidence mainly affects the Ionian coastal areas and some Tyrrhenian zones, with rates ranging from a few mm/year to over 20 mm/year. The phenomenon is associated with tectonic activity and groundwater extraction in Sibari, natural processes and hydrocarbon extraction in Crotone, and agricultural and industrial water withdrawal in Gioia Tauro [88–97]. Subsidence amplifies coastal vulnerability and threatens both archaeological heritage and modern settlements. Resulting vulnerability index values (S) range from 1 to 4, with the highest recorded in areas near the Sibari plain (Villapiana Lido, Rossano) and the Gioia Tauro plain (Palmi, San Ferdinando).

Due to Calabria's steep orography, with mountain ranges close to the coast, numerous small, steep catchments are characterized by flash floods and intense sediment transport [98]. A total of 262 catchments (>4 km 2 or of specific interest) were analyzed, estimating mean annual volumes of eroded material using the Gavrilovic model [99] in a GIS environment with morphometric, pluviometric, thermometric, and land-use data [100]. The largest catchments are the Crati (\approx 2500 km 2), Neto (\approx 1100 km 2), Mesima (\approx 800 km 2), and Lao (\approx 600 km 2). The highest fluvial sediment yields were estimated for the Lao (132,229 m 3 /year), Neto (107,877 m 3 /year), and Allaro (102,671 m 3 /year) rivers. The longshore sediment transport was estimated using the Tomasicchio et al. (2013) model [101], implemented in MATLAB and applied to meteomarine and sedimentological data from the 54 study sites. The model provided both magnitude and direction of transport, offering key insights into coastal dynamics. The results show wide spatial variability, from 2,815 m 3 /year at Villapiana Lido to 241,000 m 3 /year at Cirò Marina, confirming the strong influence of local wave climate, sediment texture, and geomorphological setting on sediment transport patterns. The resulting Sediment Transport Index (ST)—representing the balance between fluvial sediment inputs and longshore sediment removal—spans all vulnerability classes, with the highest values recorded in several Ionian and Tyrrhenian sites.

For the Coastal Defense Structures (CDS) and Port Structures (PS) indices, the obtained values fall within medium–high and medium–low vulnerability classes, respectively, where such structures are present. Satellite image analysis enabled evaluation of the type, geometry, and conservation state of coastal defenses: among the 54 analyzed sites, 29 are protected by defense structures, with protected shoreline lengths ranging from 2.5% (Belmonte Marina) to 48% (San Lucido). Identified

structures include groynes, emerged and submerged barriers, and mixed systems. A total of 24 ports were surveyed and measured relative to the 1954 shoreline; the largest is the new port of Crotone (1122 m), followed by Cetraro (489 m), Cariati (457 m), and Roccella Ionica (415 m) [102].

For the Coastal Anthropization Index (CA), all sites fall within the maximum vulnerability class, as the degree of shoreline urbanization is generally low (<20%), except for Marina di Belvedere and Sangineto Lido, which fall into the fourth class with 21% and 29.6%, respectively.

Table 10 reports the normalized overall vulnerability index values obtained for each site, calculated using Equation (3) and weighted according to the coefficients provided in Table 5, together with the corresponding vulnerability classification. The results indicate moderate vulnerability for most sites, medium-low for four Ionian and two Tyrrhenian sites, and medium-high for five Ionian, three Tyrrhenian, and two Strait of Messina sites (Figure 5).

Table 10. Normalized values of the overall coastal vulnerability index calculated for each analyzed site according to the proposed methodology.

N.	I_V	Vulnerability level	N.	I_V	Vulnerability level	N.	I_V	Vulnerability level
1	0.56	Medium	19	0.41	Medium	37	0.49	Medium
2	0.52	Medium	20	0.35	Medium - low	38	0.49	Medium
3	0.44	Medium	21	0.42	Medium	39	0.55	Medium
4	0.35	Medium - low	22	0.34	Medium - low	40	0.57	Medium
5	0.42	Medium	23	0.42	Medium	41	0.59	Medium
6	0.54	Medium	24	0.57	Medium	42	0.51	Medium
7	0.66	Medium – high	25	0.46	Medium	43	0.45	Medium
8	0.51	Medium	26	0.41	Medium	44	0.53	Medium
9	0.66	Medium – high	27	0.46	Medium	45	0.64	Medium – high
10	0.56	Medium	28	0.48	Medium	46	0.64	Medium – high
11	0.53	Medium	29	0.52	Medium	47	0.56	Medium
12	0.62	Medium – high	30	0.62	Medium – high	48	0.59	Medium
13	0.56	Medium	31	0.50	Medium	49	0.63	Medium – high
14	0.44	Medium	32	0.69	Medium – high	50	0.59	Medium
15	0.44	Medium	33	0.65	Medium – high	51	0.51	Medium
16	0.35	Medium - low	34	0.56	Medium	52	0.35	Medium - low
17	0.47	Medium	35	0.60	Medium – high	53	0.39	Medium - low
18	0.41	Medium	36	0.58	Medium	54	0.44	Medium

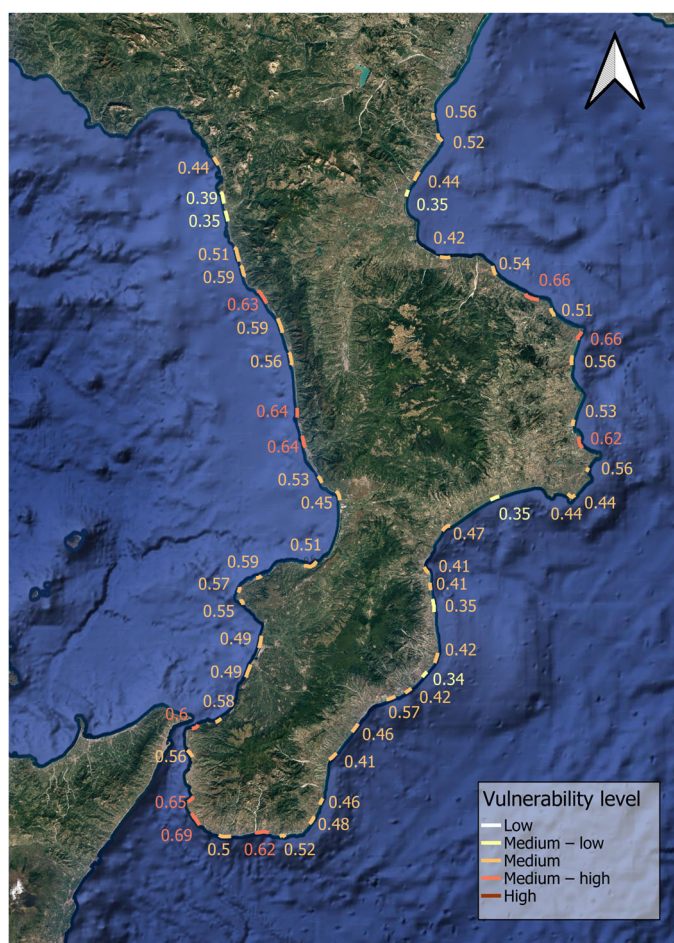


Figure 5. Vulnerability map.

3.3. Coastal Hazard-Area

For hazard-area assessment, total levels were estimated by summing the maximum contributions from wind set-up, barometric set-up, astronomical tide, wave run-up and set-up (TR = 100 years), and the projected sea-level rise under the IPCC SSP5–8.5 scenario [103]. The resulting total water levels reflect local coastal slopes, with values ranging from 3.15 m at Villapiana Lido to 7.82 m at Lazzaro. Hazard areas were delineated in a QGIS environment using 5 m-resolution regional DTMs [73], accounting for both total water level and the linear extent of each coastal segment. The mapped hazard areas range from 1.43 km² at Vibo Marina (the largest) to 0.006 km² at Isola di Capo Rizzuto–Marinella (Figure 6).



Figure 6. Example of a mapped coastal hazard area detected in Vibo Marina.

3.4. Coastal Exposure

Regarding exposure, most sites show low values of resident population within hazard zones. However, land use associated with tourism and coastal development produces high exposure scores in several areas, particularly along the Tyrrhenian coast. In particular, analysis of the resident population within the hazard area shows that almost all surveyed localities fall within the lowest exposure class, with the exception of Rossano, Gallico, and Vibo Marina. In contrast, the land use index displays a wider distribution across all five exposure classes, with maximum values observed in Caulonia Marina, Lazzaro, Pellaro, Gallico, Gizzeria Lido, Falerna Marina, and Cetraro Marina.

Table 11 presents the normalized overall exposure index values for each site, calculated using Equation (4) and weighted according to the coefficients in Table 6, together with their exposure classification. The results reveal considerable spatial variability: three sites on the Ionian coast show low exposure, while seven sites—mostly along the Tyrrhenian coast—exhibit high exposure levels (Figure 7).

Table 11. Normalized values of the overall coastal exposure index calculated for each analyzed site according to the proposed methodology.

N.	I_E	Exposure level	N.	I_E	Exposure level	N.	I_E	Exposure level
1	0.40	Medium	19	0.60	Medium – high	37	0.40	Medium
2	0.40	Medium	20	0.40	Medium	38	0.60	Medium – high
3	0.40	Medium	21	0.20	Medium - low	39	0.40	Medium
4	0.40	Medium	22	0.20	Medium - low	40	0.40	Medium
5	0.65	Medium – high	23	0.80	High	41	0.20	Medium - low
6	0.40	Medium	24	0.20	Medium - low	42	0.45	Medium
7	0.40	Medium	25	0.00	Low	43	0.80	High
8	0.60	Medium – high	26	0.20	Medium - low	44	0.80	High
9	0.40	Medium	27	0.40	Medium	45	0.20	Medium - low
10	0.20	Medium - low	28	0.40	Medium	46	0.20	Medium - low
11	0.60	Medium – high	29	0.40	Medium	47	0.20	Medium - low
12	0.60	Medium – high	30	0.40	Medium	48	0.20	Medium - low
13	0.00	Low	31	0.20	Medium - low	49	0.80	High
14	0.00	Low	32	0.80	High	50	0.40	Medium
15	0.20	Medium - low	33	0.80	High	51	0.60	Medium – high
16	0.40	Medium	34	0.85	High	52	0.60	Medium – high
17	0.20	Medium - low	35	0.20	Medium - low	53	0.60	Medium – high
18	0.20	Medium - low	36	0.20	Medium - low	54	0.20	Medium - low

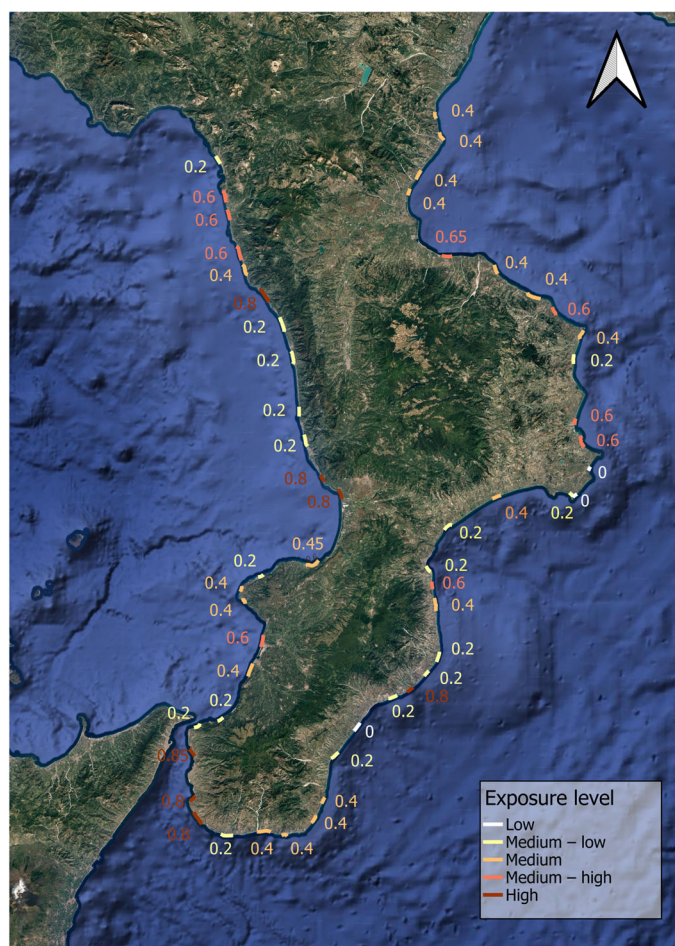


Figure 7. Exposure map.

3.5. Coastal Risk

The integration of the three components—hazard, vulnerability, and exposure—resulted in the definition of the coastal risk index (I_R), providing an articulated overview of coastal risk across Calabria. The results — shown in Table 12 — identify nine sites with low risk (all located along the Ionian coast), 29 with medium–low risk, 14 with medium risk, and two sites with medium–high risk (Falerna Marina and Cetraro Marina), both situated along the Tyrrhenian coast and characterized by high urbanization (Figure 8). These findings highlight that coastal risk is not uniformly distributed but depends on the combined influence of natural conditions and anthropogenic pressure.

Table 12. Values of the coastal risk index calculated for each analyzed site according to the proposed methodology.

N.	I_R	Risk level	N.	I_R	Risk level	N.	I_R	Risk level
1	0.10	Medium - low	19	0.12	Medium - low	37	0.14	Medium - low
2	0.09	Medium - low	20	0.08	Medium - low	38	0.18	Medium
3	0.08	Medium - low	21	0.05	Low	39	0.13	Medium - low
4	0.06	Medium - low	22	0.04	Low	40	0.16	Medium
5	0.12	Medium - low	23	0.20	Medium	41	0.09	Medium - low
6	0.10	Medium - low	24	0.07	Medium - low	42	0.14	Medium - low
7	0.12	Medium - low	25	0.00	Low	43	0.21	Medium
8	0.14	Medium - low	26	0.05	Low	44	0.30	Medium – high
9	0.15	Medium	27	0.12	Medium - low	45	0.09	Medium - low
10	0.06	Medium - low	28	0.12	Medium - low	46	0.09	Medium - low

11	0.18	Medium	29	0.10	Medium - low	47	0.08	Medium - low
12	0.17	Medium	30	0.12	Medium - low	48	0.09	Medium - low
13	0.00	Low	31	0.05	Low	49	0.36	Medium - high
14	0.00	Low	32	0.26	Medium	50	0.17	Medium
15	0.04	Low	33	0.25	Medium	51	0.22	Medium
16	0.08	Medium - low	34	0.24	Medium	52	0.15	Medium
17	0.06	Medium - low	35	0.09	Medium - low	53	0.17	Medium
18	0.04	Low	36	0.07	Medium - low	54	0.05	Medium - low

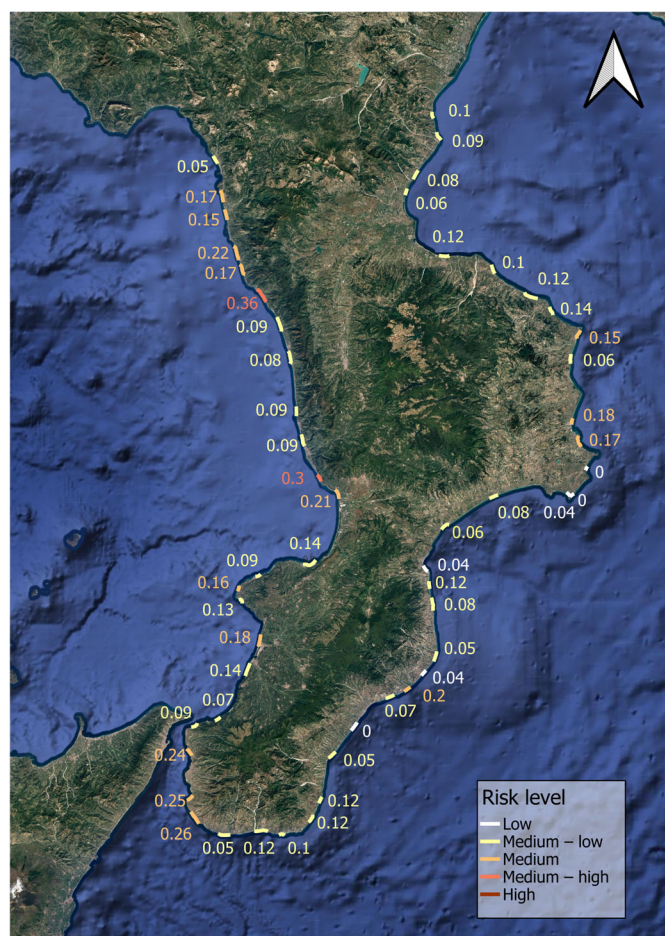


Figure 8. Risk map.

4. Discussion

The results of this study highlight the complex and spatially variable nature of coastal erosion risk along the Calabrian coast, which is shaped by the interplay between physical processes, geomorphological settings, and anthropogenic pressures.

The analysis of hazard variables revealed that sea-level rise (SLR) represents a critical and non-negligible driver, classifying all sites within the highest hazard class. Although SLR variations at the regional scale are limited, its cumulative effect over time is expected to exacerbate both erosion and inundation hazards, emphasizing the importance of integrating climate projections into regional planning. The wave climate emerged as the dominant forcing agent, particularly along the Tyrrhenian coast and within the Strait of Messina, where energetic sea states, extended fetch, and steep seabed slopes combine to increase run-up and coastal retreat potential. Conversely, the Ionian sector exhibited more complex exposure conditions due to multiple wave approach directions and a broader spectrum of energy fluxes. In contrast, wind and tidal indices proved to be less significant,

consistent with the region's microtidal regime and the limited incidence of aeolian sediment transport. Moreover, the hazard associated with marine currents is generally minimal, except in the Strait of Messina. Consequently, the combined influence of wave dynamics and coastal morphology accounts for most of the spatial variability in coastal hazard.

Vulnerability patterns are more heterogeneous and closely tied to geomorphological and anthropogenic characteristics. The predominance of sandy beaches, high subsidence rates in specific plains (Sibari and Gioia Tauro), and the widespread degradation or loss of natural buffers such as dunes and vegetation contribute to elevated vulnerability levels across much of the region. The presence of coastal defense structures and ports, while locally mitigating erosion, often disrupts sediment transport and induces secondary imbalances. Notably, the contrast between heavily urbanized Tyrrhenian sectors and less developed Ionian sectors underscores the strong role of human pressure in amplifying coastal susceptibility [104].

The exposure indices show pronounced variability. In most localities, population density within hazard zones remains low, resulting in limited exposure scores for the population index. However, land-use patterns significantly increase exposure in areas with high levels of urbanization or concentration of port and tourism infrastructures — notably in Falerna, Cetraro and Pellarolo. This indicates that exposure is not solely related to permanent population density but rather to the intensity of anthropogenic pressure and coastal land use, with critical conditions where such pressures coincide with unstable natural settings.

The overall risk synthesis places most localities within low to medium-low risk classes, predominantly along the Ionian coast, where human pressures have historically been less intense. However, several critical hotspots emerge: Falerna Marina and Cetraro Marina, both along the Tyrrhenian coast, exhibit medium-high risk levels driven by the combination of high wave hazard, strong urbanization, and dense coastal infrastructure. These criticalities, consistent with the findings of several previous studies that have highlighted the vulnerability and shoreline retreat of the Tyrrhenian sector [105–108], confirm the need for integrated risk management strategies that address not only physical factors but also spatial planning and the mitigation of anthropogenic pressures.

5. Conclusions

This study addressed the need for a unified and comprehensive framework for coastal risk assessment, responding to the current fragmentation of methods and indicators at both national and international scales. A new index-based methodology was therefore developed to evaluate coastal erosion risk, designed to integrate all key physical, geomorphological, climatic, and anthropogenic factors influencing coastal dynamics. Moreover, the proposed methodology is multi-scale and multi-risk by design. It can be applied at various territorial levels — from local to regional — and adapted to different coastal contexts by recalibrating classification thresholds and weighting factors. Furthermore, because most variables also influence coastal flooding, the same framework can be used to evaluate flood risk, adopting a different weighting scheme.

The methodology was applied to 54 representative sites along the Calabrian coast (32 on the Ionian side, 3 within the Strait of Messina, and 19 along the Tyrrhenian coast), demonstrating its robustness and adaptability. The results indicate that 16% of the analyzed sites fall within the low-risk class, 54% within medium-low, 26% within medium, and 4% within medium-high risk. The analysis reveals pronounced spatial variability in coastal risk across Calabria, with the Tyrrhenian sector exhibiting the highest levels due to the combined influence of an energetic wave climate and increasing anthropogenic pressure. These contrasts highlight the need for management strategies tailored to local coastal conditions. Overall, the findings confirm the robustness and applicability of the proposed methodology in capturing the complexity of coastal erosion dynamics in Calabria.

A key advantage of this approach lies in its integration within a GIS environment, ensuring transparency, reproducibility, and usability for public administrations and stakeholders. Future developments include the creation of an open-access GIS plug-in to facilitate the input of local data and the automatic generation of hazard, vulnerability, exposure, and risk maps.

In conclusion, the proposed methodology represents an effective and flexible tool for integrated coastal risk management. Its accessibility and adaptability make it particularly valuable for stakeholders and public administrations, supporting evidence-based prioritization of coastal defense measures and sustainable spatial planning.

Author Contributions: Conceptualization, G.C.B., G.B. and G.F.; methodology, G.C.B.; software, G.C.B., G.F. and G.M.; validation, G.C.B., G.B. and G.F.; formal analysis, G.C.B. and G.F.; investigation, G.C.B. and G.F.; resources, G.C.B., G.F. and G.M.; data curation, G.C.B. and G.F.; writing—original draft preparation, G.C.B.; writing—review and editing, G.C.B., G.B., G.F. and G.M.; visualization, G.C.B.; supervision, G.B.; project administration, G.B. All authors have read and agreed to the published version of the manuscript.

Funding: This research received no external funding.

Institutional Review Board Statement: Not applicable.

Informed Consent Statement: Not applicable.

Data Availability Statement: Not applicable.

Conflicts of Interest: The authors declare no conflicts of interest. The funders had no role in the design of the study; in the collection, analyses, or interpretation of data; in the writing of the manuscript; or in the decision to publish the results.

References

1. McLaughlin, S.; Cooper, J.A.G. A multi-scale coastal vulnerability index: A tool for coastal managers? *Environ. Hazards* **2010**, *9*, 233–248. <https://doi.org/10.3763/ehaz.2010.0052>
2. Ramieri, E.; Hartley, A.; Barbanti, A.; Santos, F.D.; Gomes, A.; Hilden, M.; Santini, M. Methods for assessing coastal vulnerability to climate change. *ETC CCA Tech. Pap.* **2011**, *1*, 1–93.
3. Komar, P.D. Coastal erosion—underlying factors and human impacts. *Shore & Beach* **2000**, *68*, 3–16.
4. Barbaro, G.; Foti, G.; Sicilia, C.L. Coastal erosion in the South of Italy. *Disaster Adv.* **2014**, *7*, 37–42.
5. Vousdoukas, M.I.; Ranasinghe, R.; Mentaschi, L.; Plomaritis, T.A.; Athanasiou, P.; Luijendijk, A.; Feyen, L. Sandy coastlines under threat of erosion. *Nat. Clim. Change* **2020**, *10*, 260–263. <https://doi.org/10.1038/s41558-020-0697-0>
6. Magalhães Filho, L.N.L.; Roebeling, P.C.; Costa, L.F.C.; Lima, L.T. Ecosystem services values at risk in the Atlantic coastal zone due to sea-level rise and socioeconomic development. *Ecosyst. Serv.* **2022**, *58*, 101492. <https://doi.org/10.1016/j.ecoser.2022.101492>
7. Andreadis, O.; Chatzipavlis, A.; Hasiotis, T.; Monioudi, I.; Manoutsoglou, E.; Velegrakis, A. Assessment of and adaptation to beach erosion in islands: An integrated approach. *J. Mar. Sci. Eng.* **2021**, *9*, 859. <https://doi.org/10.3390/jmse9080859>
8. Ortega, A.Y.; Díaz, L.J.O.; Cueto, J.E. Assessment and management of coastal erosion in the marine protected area of the Rosario Island archipelago (Colombian Caribbean). *Ocean Coast. Manag.* **2023**, *239*, 106605. <https://doi.org/10.1016/j.ocecoaman.2023.106605>
9. Gornitz, V. Global coastal hazards from future sea level rise. *Glob. Planet. Change* **1991**, *3*, 379–398. [https://doi.org/10.1016/0031-0182\(91\)90173-O](https://doi.org/10.1016/0031-0182(91)90173-O)
10. Thieler, E.R.; Hammar-Klose, E. National Assessment of Coastal Vulnerability to Sea Level Rise: Preliminary Results for the U.S. Atlantic Coast. *U.S. Geological Survey Open-File Report 99-593*; U.S. Geological Survey: Washington, DC, USA, 1999.
11. Viavattene, C.; Jiménez, J. A.; Ferreira, O.; Priest, S.; Owen, D.; McCall, R. Finding coastal hotspots of risk at the regional scale: the Coastal Risk Assessment Framework. *Coast. Eng.* **2017**. <https://doi.org/10.1016/j.coastaleng.2017.09.002>
12. Satta, A.; Snoussi, M.; Puddu, M.; Flayou, L.; Hoult, R. An index-based method to assess risks of climate-related hazards in coastal zones: the case of Tetouan. *Estuar. Coast. Shelf Sci.* **2016**, *175*, 93–105. <https://doi.org/10.1016/j.ecss.2016.03.021>

13. Satta, A.; Puddu, M.; Venturini, S.; Giupponi, C. Assessment of coastal risks to climate change related impacts at regional scale: the case of Mediterranean region. *Int. J. Disaster Risk Reduct.* **2017**, *24*, 284–296. <https://doi.org/10.1016/j.ijdrr.2017.06.018>
14. Narra, P.; Coelho, C.; Sancho, F.; Palalane, J. CERA: an open-source tool for coastal erosion risk assessment. *Ocean Coast. Manag.* **2017**, *142*, 1–14. <https://doi.org/10.1016/j.ocecoaman.2017.03.013>
15. Greco, M.; Martino, G. Assessment of maritime erosion index for Ionian-Lucanian coast. In *Engineering Geology for Society and Territory*; Springer: Cham, Switzerland, 2014; Volume 4, pp. 41–44. https://doi.org/10.1007/978-3-319-08660-6_8
16. Barbaro, G. Master Plan of solutions to mitigate the risk of coastal erosion in Calabria (Italy), a case study. *Ocean Coast. Manag.* **2016**, *132*, 24–35. <https://doi.org/10.1016/j.ocecoaman.2016.08.001>
17. Benassai, G.; Di Paola, G.; Aucelli, P.P.C. Coastal risk assessment of a micro-tidal littoral plain in response to sea level rise. *Ocean Coast. Manag.* **2015**, *104*, 22–35. <https://doi.org/10.1016/j.ocecoaman.2014.11.015>
18. Aucelli, P.P.C.; Di Paola, G.; Rizzo, A.; Rosskopf, C.M. Rischio all’erosione costiera del settore meridionale della costa molisana. *Studi Costieri* **2017**, *26*, 107–122.
19. Armaroli, C.; Duo, E. Validation of the coastal storm risk assessment framework along the Emilia-Romagna coast. *Coast. Eng.* **2018**, *134*, 159–167. <https://doi.org/10.1016/j.coastaleng.2017.08.014>
20. Pantusa, D.; D’Alessandro F.; Riefolo L.; Principato F.; Tomasicchio G. Application of a coastal vulnerability index. A case study along the Apulian Coastline, Italy. *Water* **2018**, *10*, 1218. <https://doi.org/10.3390/w10091218>
21. Ciccarelli, D.; Pinna, M. S.; Alquini, F.; Cogoni, D.; Ruocco, M.; Bacchetta, G.; Sarti G.; Fenu, G. Development of a coastal dune vulnerability index for Mediterranean ecosystems: A useful tool for coastal managers?. *Estuar. Coast. Shelf Sci.* **2017**, *187*, 84–95. <https://doi.org/10.1016/j.ecss.2016.12.008>
22. Torresan, S.; Critto, A.; Rizzi, J.; Marcomini, A. Assessment of coastal vulnerability to climate change hazards at the regional scale: the case study of the North Adriatic Sea. *Nat. Hazards Earth Syst. Sci.* **2012**, *12*, 2347–2368. <https://doi.org/10.5194/nhess-12-2347-2012>
23. Silva, S. F.; Martinho, M.; Capitão, R.; Reis, T.; Fortes, C. J.; Ferreira, J. C. An index-based method for coastal-flood risk assessment in low-lying areas (Costa de Caparica, Portugal). *Ocean Coast. Manag.* **2017**, *144*, 90–104. <https://doi.org/10.1016/j.ocecoaman.2017.04.010>
24. Mavromatidi, A.; Briche, E.; Claeys, C. Mapping and analyzing socio-environmental vulnerability to coastal hazards induced by climate change: an application to coastal Mediterranean cities in France. *Cities* **2018**, *72*, 189–200. <https://doi.org/10.1016/j.cities.2017.08.007>
25. Fitton, J.M.; Hansom, J.D.; Rennie, A.F. A national coastal erosion susceptibility model for Scotland. *Ocean Coast. Manag.* **2016**, *132*, 80–89. <https://doi.org/10.1016/j.ocecoaman.2016.08.018>
26. Kantamaneni, K.; Phillips, M.; Thomas, T.; Jenkins, R. Assessing coastal vulnerability: Development of a combined physical and economic index. *Ocean Coast. Manag.* **2018**, *158*, 164–175. <https://doi.org/10.1016/j.ocecoaman.2018.03.039>
27. Mohamed, S. A. Coastal vulnerability assessment using GIS-Based multicriteria analysis of Alexandria-northwestern Nile Delta, Egypt. *J. Afr. Earth Sci.* **2020**, *163*, 103751. <https://doi.org/10.1016/j.jafrearsci.2020.103751>
28. Rehman, S.; Jahangir, S.; Azhoni, A. GIS based coastal vulnerability assessment and adaptation barriers to coastal regulations in Dakshina Kannada district, India. *Reg. Stud. Mar. Sci.* **2022**, *55*, 102509. <https://doi.org/10.1016/j.rsma.2022.102509>
29. Roy, S.; Pandit, S.; Papia, M.; Rahman, M. M.; Ocampo, J. C. O. R.; Razi, M. A.; ... Hossain, M. S. Coastal erosion risk assessment in the dynamic estuary: The Meghna estuary case of Bangladesh coast. *Int. J. Disaster Risk Reduct.* **2021**, *61*, 102364. <https://doi.org/10.1016/j.ijdrr.2021.102364>
30. Thirumurthy, S.; Jayanthi, M.; Samynathan, M.; Duraisamy, M.; Kabiraj, S.; Anbazhahan, N. Multi-criteria coastal environmental vulnerability assessment using analytic hierarchy process based uncertainty analysis integrated into GIS. *J. Environ. Manag.* **2022**, *313*, 114941. <https://doi.org/10.1016/j.jenvman.2022.114941>

31. Ariffin, E. H.; Mathew, M. J.; Roslee, A.; Ismailluddin, A.; Yun, L. S.; Putra, A. B.; ... Lee, L. H. A multi-hazards coastal vulnerability index of the east coast of Peninsular Malaysia. *Int. J. Disaster Risk Reduct.* **2023**, *84*, 103484. <https://doi.org/10.1016/j.ijdrr.2022.103484>
32. Barzehkar, M.; Parnell, K.; Soomere, T. Extending multi-criteria coastal vulnerability assessment to low-lying inland areas: examples from Estonia, eastern Baltic Sea. *Estuar. Coast. Shelf Sci.* **2024**, *311*, 109014. <https://doi.org/10.1016/j.ecss.2024.109014>
33. Ahmed, M.A.; Sridharan, B.; Saha, N.; Sannasiraj, S. A.; Kuiry, S. N. Assessment of coastal vulnerability for extreme events. *Int. J. Disaster Risk Reduct.* **2022**, *82*, 103341. <https://doi.org/10.1016/j.ijdrr.2022.103341>
34. Hossain, S.A.; Mondal, I.; Thakur, S.; Al-Quraishi, A. M. F. Coastal vulnerability assessment of India's Purba Medinipur-Balasore coastal stretch: A comparative study using empirical models. *Int. J. Disaster Risk Reduct.* **2022**, *77*, 103065. <https://doi.org/10.1016/j.ijdrr.2022.103065>
35. Kovaleva, O.; Sergeev, A.; Ryabchuk, D. Coastal vulnerability index as a tool for current state assessment and anthropogenic activity planning for the Eastern Gulf of Finland coastal zone (the Baltic Sea). *Appl. Geogr.* **2022**, *143*, 102710. <https://doi.org/10.1016/j.apgeog.2022.102710>
36. Muzirafuti, A.; Theocharidis, C. Coastal Vulnerability Index Assessment Along the Coastline of Casablanca Using Remote Sensing and GIS Techniques. *Remote Sens.* **2025**, *17*, 3370. <https://doi.org/10.3390/rs17193370>
37. Nativí-Merchán, S.; Caiza-Quinga, R.; Saltos-Andrade, I.; Martillo-Bustamante, C.; Andrade-García, G.; Quiñonez, M.; ... Cedeño, J. Coastal erosion assessment using remote sensing and computational numerical model. Case of study: Libertador Bolívar, Ecuador. *Ocean Coast. Manag.* **2021**, *214*, 105894. <https://doi.org/10.1016/j.ocecoaman.2021.105894>
38. Rocha, C.; Antunes, C.; Catita, C. Coastal indices to assess sea-level rise impacts-A brief review of the last decade. *Ocean Coast. Manag.* **2023**, *237*, 106536. <https://doi.org/10.1016/j.ocecoaman.2023.106536>
39. Bianco, F.; García-Ayllón, S. Coastal resilience potential as an indicator of social and morphological vulnerability to beach management. *Estuar. Coast. Shelf Sci.* **2021**, *253*, 107290. <https://doi.org/10.1016/j.ecss.2021.107290>
40. Godwyn-Paulson, P.; Jonathan, M. P.; Rodríguez-Espinosa, P. F.; Rahaman, S. A.; Roy, P. D.; Muthusankar, G.; Lakshumanan, C. Multi-hazard risk assessment of coastal municipalities of Oaxaca, Southwestern Mexico: An index based remote sensing and geospatial technique. *Int. J. Disaster Risk Reduct.* **2022**, *77*, 103041. <https://doi.org/10.1016/j.ijdrr.2022.103041>
41. Laino, E.; Iglesias, G. Beyond coastal hazards: A comprehensive methodology for the assessment of climate-related hazards in European coastal cities. *Ocean Coast. Manag.* **2024**, *257*, 107343. <https://doi.org/10.1016/j.ocecoaman.2024.107343>
42. Bruno, M.F.; Motta Zanin, G.; Barbanente, A.; Damiani, L. Understanding the cognitive components of coastal risk assessment. *J. Mar. Sci. Eng.* **2021**, *9*, 780. <https://doi.org/10.3390/jmse9070780>
43. Manno, G.; Re, C.L.; Basile, M.; Ciraolo, G. A new shoreline change assessment approach for erosion management strategies. *Ocean Coast. Manag.* **2022**, *225*, 106226. <https://doi.org/10.1016/j.ocecoaman.2022.106226>
44. De Araujo Queiroz, H. A.; Gonçalves, R. M.; Mishra, M. Characterizing global satellite-based indicators for coastal vulnerability to erosion management as exemplified by a regional level analysis from Northeast Brazil. *Sci. Total Environ.* **2022**, *817*, 152849. <https://doi.org/10.1016/j.scitotenv.2021.152849>
45. Ennouali, Z.; Fannassi, Y.; Lahssini, G.; Benmohammadi, A.; Masria, A. Mapping coastal vulnerability using machine learning algorithms: A case study at North coastline of Sebou estuary, Morocco. *Reg. Stud. Mar. Sci.* **2023**, *60*, 102829. <https://doi.org/10.1016/j.rsma.2023.102829>
46. Townend, I. H.; French, J. R.; Nicholls, R. J.; Brown, S.; Carpenter, S.; Haigh, I. D.; ... Tompkins, E. L. Operationalising coastal resilience to flood and erosion hazard: A demonstration for England. *Sci. Total Environ.* **2021**, *783*, 146880. <https://doi.org/10.1016/j.scitotenv.2021.146880>
47. Unguendoli, S.; Biolchi, L. G.; Aguzzi, M.; Pillai, U. P. A.; Alessandri, J.; Valentini, A. A modeling application of integrated nature based solutions (NBS) for coastal erosion and flooding mitigation in the Emilia-Romagna coastline (Northeast Italy). *Sci. Total Environ.* **2023**, *867*, 161357. <https://doi.org/10.1016/j.scitotenv.2022.161357>

48. Paxton, A. B.; Riley, T. N.; Steenrod, C. L.; Puckett, B. J.; Alemu I, J. B.; Paliotti, S. T.; ... Silliman, B. R. Evidence on the performance of nature-based solutions interventions for coastal protection in biogenic, shallow ecosystems: a systematic map. *Environ. Evid.* **2024**, *13*, 28. <https://doi.org/10.1186/s13750-024-00350-5>

49. Berre, I.L.; Meur-Ferec, C. Systemic vulnerability of coastal territories to erosion and marine flooding: A conceptual and methodological approach applied to Brittany (France). *Int. J. Disaster Risk Reduct.* **2022**, *78*, 103143. <https://doi.org/10.1016/j.ijdrr.2022.103122>

50. Mandal, K.; Dey, P. Coastal vulnerability analysis and RIDIT scoring of socio-economic vulnerability indicators—A case of Jagatsinghpur, Odisha. *Int. J. Disaster Risk Reduct.* **2022**, *79*, 103143. <https://doi.org/10.1016/j.ijdrr.2022.103143>

51. Mucerino, L.; Albarella, M.; Carpi, L.; Besio, G.; Benedetti, A.; Corradi, N.; ... & Ferrari, M. Coastal exposure assessment on Bonassola bay. *Ocean Coast. Manag.* **2019**, *167*, 20–31. <https://doi.org/10.1016/j.ocecoaman.2018.09.015>

52. Pendleton, E.A.; Thieler, R.S.; Williams, J. Coastal vulnerability assessment of Fire Island National seashore (FIIS) to Sea level Rise. *USGS Open File Rep.* **2004**, *03*, 439.

53. Hayes, M. O. Barrier island morphology as a function of tidal and wave regime. In *Barrier Islands*; Leatherman, S.P., Ed.; Academic Press: New York, NY, USA, 1979; Volume 1, pp. 27.

54. Bagnold, R.A. *The Physics of Blown Sand and Desert Dunes*; William Morrow & Co.: New York, NY, USA, 1941.

55. Hsu, S. Computing eolian sand transport from routine weather data. *Coast. Eng. Proc.* **1974**, *1*(14), 94. <https://doi.org/10.1061/9780872621138.097>

56. Stockdon, H. F.; Holman, R. A.; Howd, P. A.; Sallenger Jr, A. H. Empirical parameterization of setup, swash, and runup. *Coast. Eng.* **2006**, *53*, 573–588. <https://doi.org/10.1016/j.coastaleng.2005.12.005>

57. Ferreira, O.; Plomaritis, T.A.; Costas, S. Process-based indicators to assess storm induced coastal hazard. *Earth-Sci. Rev.* **2017**, *173*, 159–167. <https://doi.org/10.1016/j.earscirev.2017.07.010>

58. Foti, G.; Barbaro, G.; Barillà, G.C.; Mancuso, P.; Puntorieri, P. Shoreline evolutionary trends along calabrian coasts: Causes and classification. *Front. Mar. Sci.* **2022**, *9*, 846914. <https://doi.org/10.3389/fmars.2022.846914>

59. Mendoza, E.; Odériz, I.; Martínez, M.L.; Silva, R. Measurements and modelling of small scale processes of vegetation preventing dune erosion. *J. Coast. Res.* **2017**, *77*, 19–27.

60. Gedan, K.B.; Kirwan, M.L.; Wolanski, E.; Barbier, E. B.; Silliman, B. R. The present and future role of coastal wetland vegetation in protecting shorelines: answering recent challenges to the paradigm. *Clim. Change* **2011**, *106*, 7–29. <https://doi.org/10.1007/s10584-010-0003-7>

61. Feagin, R.A.; Furman, M.; Salgado, K.; Martinez, M. L.; Innocenti, R. A.; Eubanks, K.; ... Silva, R. The role of beach and sand dune vegetation in mediating wave run up erosion. *Estuar. Coast. Shelf Sci.* **2019**, *219*, 97–106. <https://doi.org/10.1016/j.ecss.2019.01.018>

62. Boudouresque, C.F.; Bernard, G.; Bonhomme, P.; Charbonnel, E.; Diviacco, G.; Meinesz, A.; Pergent, G.; Pergent-Martini, C.; Ruitton, S.; Tunesi, L. *Protection and Conservation of Posidonia Oceanica Meadows*; RAC/SPA: Tunis, Tunisia, 2012.

63. Trogu, D.; Simeone, S.; Ruju, A.; Porta, M.; Ibba, A.; DeMuro, S. A Four-Year Video Monitoring Analysis of the Posidonia oceanica Banquette Dynamic: A Case Study from an Urban Microtidal Mediterranean Beach (Poetto Beach, Southern Sardinia, Italy). *J. Mar. Sci. Eng.* **2023**, *11*, 2376. <https://doi.org/10.3390/jmse11122376>

64. Astudillo-Gutierrez, C.; Rabionet, I.C.; Garcia, V.G.; Pedrico, J. P. S.; Conejo, A. S. A. Study of velocity changes induced by Posidonia oceanica surrogate and sediment transport implications. *J. Mar. Sci. Eng.* **2024**, *12*, 569. <https://doi.org/10.3390/jmse12040569>

65. Sekovski, I.; Del Río, L.; Armaroli, C. Development of a coastal vulnerability index using analytical hierarchy process and application to Ravenna province (Italy). *Ocean Coast. Manag.* **2020**, *183*, 104982. <https://doi.org/10.1016/j.ocecoaman.2019.104982>

66. Sabatier, F.; Anthony, E.J.; Héquette, A.; Suanez, S.; Musereau, J.; Ruz, M.H.; Regnault, H. Morphodynamics of beach/dune systems: Examples from the coast of France. *Géomorphologie: Relief, Processus, Environnement* **2009**, *15*(1), 3–22. <https://doi.org/10.4000/geomorphologie.7461>

67. Sancho, F.; Abreu, T.; D'Alessandro, F.; Tomasicchio, G. R.; Silva, P. A. Surf hydrodynamics in front of collapsing coastal dunes. *J. Coast. Res.* **2011**, *144*–148.

68. Cozzolino, D.; Greggio, N.; Antonellini, M.; Giambastiani, B. M. S. Natural and anthropogenic factors affecting freshwater lenses in coastal dunes of the Adriatic coast. *J. Hydrol.* **2017**, *551*, 804–818. <https://doi.org/10.1016/j.jhydrol.2017.04.039>

69. Van der Meer, J. W. Static and dynamic stability of loose material. In *Coastal Protection*; Balkema: Rotterdam, The Netherlands, 1990; pp. 157–195.

70. Salman, A.; Lombardo, S.; Doody, P. *Living with Coastal Erosion in Europe: Sediment and Space for Sustainability*; EUROSION Project Report; European Commission: Brussels, Belgium, 2004.

71. ISTAT. Censimento permanente. Available online: <http://dati-censimentipermanenti.istat.it/> (accessed on 10 October 2024).

72. Corine Land Cover. Available online: <https://www.isprambiente.gov.it/it/attivita/suolo-e-territorio/suolo/copertura-del-suolo/corine-land-cover> (accessed on 15 July 2024).

73. Calabrian Geoportal. Available online: <https://geoportale.regione.calabria.it/> (accessed on 18 December 2024).

74. ISPRA. Direttiva Alluvioni—Documenti. Available online: https://gn.mase.gov.it/portale/documents/d/geoportale-mase/documento_definitivo_indirizzi_operativi_direttiva_alluvioni_gen_13 (accessed on 21 March 2024).

75. ISPRA. Mappatura del rischio costiero; ISPRA: Rome, Italy, 2007.

76. Hamlington, B. D.; Bellas-Manley, A.; Willis, J. K.; Fournier, S.; Vinogradova, N.; Nerem, R. S.; ... Kopp, R. The rate of global sea level rise doubled during the past three decades. *Commun. Earth Environ.* **2024**, *5*, 601. <https://doi.org/10.1038/s43247-024-01761-5>

77. MeteOcean Group – DICCA, University of Genoa. Available online: <https://forecast.meteocean.science/> (accessed on 24 April 2025).

78. National tidal network – RMN (ISPRA). Available online: <https://www.mareografico.it/> (accessed on 21 May 2025).

79. Sannino, G.; Carillo, A.; Pisacane, G.; Naranjo, C. On the relevance of tidal forcing in modeling the Mediterranean thermohaline circulation. *Prog. Oceanogr.* **2015**, *134*, 304–329. <https://doi.org/10.1016/j.pocean.2015.03.002>

80. Mosetti F. Some News on the Currents in the Straits of Messina. *Boll. Oceanol. Teor. Appl.* **1988**, *6*, 119–201.

81. Coiro, D.P.; Lioniello, F.; Troise, G. *Misura del profilo di corrente marina nello stretto di Messina ai fini della stima della produzione di energia*. ENEA Report RdS/2013/087, 2013.

82. Foti, G.; Barbaro, G.; Besio, G.; Barillà, G. C.; Mancuso, P.; Puntorieri, P. Wave climate along Calabrian coasts. *Climate* **2022**, *10*, 80. <https://doi.org/10.3390/cli10060080>

83. Regione Calabria. *Indagine conoscitiva dello stato delle coste calabresi, predisposizione di una banca dati dell'evoluzione del litorale e individuazione delle aree a rischio e delle tipologie di intervento studi su aree campione e previsione delle relative opere di difesa*. TECHNITAL/IDROTEC/ CONSORZIO OKEANOS, 2003.

84. EMODnet Digital Bathymetry (DTM 2020). EMODnet Bathymetry Consortium. (accessed on 21 June 2024). <https://doi.org/10.12770/bb6a87dd-e579-4036-abe1-e649cea9881a>

85. Italian Geoportal. Available online: <https://gn.mase.gov.it/portale/home> (accessed on 18 December 2024).

86. MEDISEH Project. Available online: <https://imbriw.hcmr.gr/mediseh/> (accessed on 24 June 2024).

87. Foti, G.; Barbaro, G.; Barillà, G.C.; Frega, F. Effects of anthropogenic pressures on dune systems. Case study: Calabria (Italy). *J. Mar. Sci. Eng.* **2021**, *10*, 10. <https://doi.org/10.3390/jmse10010010>

88. Gisotti, G. A Case of Induced Subsidence for Extraction of Salt by Hydrosolution. In *Proc. 4th Int. Symp. Land Subsidence*, Houston, TX, USA, 1987; pp. 12–17.

89. Cherubini, C.; Cotecchia, V.; Pagliarulo, R. Subsidence in the Sybaris Plain (Italy). In *Land Subsidence. Proceedings of the Sixth International Symposium on Land Subsidence*, Volume 1, 2000; pp. 3–15.

90. Raspini, F.; Cigna, F.; Moretti, S. Multi-temporal mapping of land subsidence at basin scale exploiting Persistent Scatterer Interferometry: Case study of Gioia Tauro plain (Italy). *J. Maps* **2012**, *8*, 514–524. <https://doi.org/10.1080/17445647.2012.743440>

91. Cafaro, F.; Cotecchia, F.; Lenti, V. Interpretation and modelling of the subsidence at the archaeological site of Sybaris (Southern Italy). In *Geotechnical Engineering for the Preservation of Monuments*; Taylor & Francis: London, UK, 2013; pp. 199–206.

92. Pepe, F.; Bertotti, G.; Ferranti, L.; Sacchi, M.; Collura, A. M.; Passaro, S.; Sulli, A. Pattern and rate of post-20 ka vertical tectonic motion around the Capo Vaticano Promontory (W Calabria, Italy) based on offshore geomorphological indicators. *Quat. Int.* **2014**, *332*, 85–98. <https://doi.org/10.1016/j.quaint.2013.11.012>

93. Cianflone, G.; Tolomei, C.; Brunori, C.A.; Dominici, R. InSAR time series analysis of natural and anthropogenic coastal plain subsidence: The case of Sibari (Southern Italy). *Remote Sens.* **2015**, *7*, 16004–16023. <https://doi.org/10.3390/rs71215812>

94. Cianflone, G.; Tolomei, C.; Brunori, C.A.; Dominici, R. Preliminary study of the surface ground displacements in the Crati Valley (Calabria) by means of InSAR data. *Rend. Online Soc. Geol. Ital.* **2015**, *33*, 20–23. <https://doi.org/10.3301/ROL.2015.05>

95. Cigna, F.; Confuorto, P.; Novellino, A.; Tapete, D.; Di Martire, D.; Ramondini, M.; Sowter, A. 25 Years of Satellite InSAR Monitoring of Ground Instability and Coastal Geohazards in the Archaeological Site of Capo Colonna, Italy. In *Proceedings of the SAR Image Analysis, Modeling, and Techniques XVI*, Edinburgh, UK, 26–29 September 2016; SPIE: Bellingham, WA, USA, 2016; Volume 10003, pp. 130–143. <https://doi.org/10.1117/12.2242095>

96. Confuorto, P.; Plank, S.; Novellino, A.; Tessitore, S.; Ramondini, M. Implementation of DInSAR Methods for the Monitoring of the Archaeological Site of Hera Lacinia in Crotone (Southern Italy). *Rend. Online Soc. Geol. Ital.* **2016**, *41*, 231–234. <https://doi.org/10.3301/ROL.2016.136>

97. Cigna, F.; Tapete, D. Sentinel-1 big data processing with P-SBAS InSAR in the geohazards exploitation platform: An experiment on coastal land subsidence and landslides in Italy. *Remote Sens.* **2021**, *13*, 885. <https://doi.org/10.3390/rs13050885>

98. Foti, G.; Barbaro, G.; Bombino, G.; Barillà, G. C.; Mancuso, P.; Puntorieri, P. River transport in Calabrian rivers. In *New Metropolitan Perspectives*; Springer: Cham, Switzerland, 2022; pp. 66–74. https://doi.org/10.1007/978-3-031-06825-6_7

99. Gavrilovic, S. Méthode de la classification des bassins torrentiels et équations nouvelles pour le calcul des hautes eaux et du débit solide. *Vadopriveda* 1959, Belgrade, Serbia.

100. Calabria Multi-Risk Functional Center. Available online: <http://www.cfd.calabria.it/> (accessed on 14 April 2025).

101. Tomasicchio, G.R.; D'Alessandro, F.; Barbaro, G.; Malara, G. General longshore transport model. *Coast. Eng.* **2013**, *71*, 28–36. <https://doi.org/10.1016/j.coastaleng.2012.07.004>

102. Foti, G.; Barbaro, G.; Barillà, G.C.; Mancuso, P. Shoreline changes due to the construction of ports: case study—Calabria (Italy). *J. Mar. Sci. Eng.* **2023**, *11*, 2382. <https://doi.org/10.3390/jmse11122382>

103. Sea Level Projection Tool – NASA. Available online: <https://sealevel.nasa.gov/ipcc-ar6-sea-level-projection-tool> (accessed on 15 May 2024).

104. Foti, G.; Barbaro, G.; Barillà, G.C.; Mancuso, P.; Puntorieri, P. Shoreline erosion due to anthropogenic pressure in Calabria (Italy). *Eur. J. Remote Sens.* **2023**, *56*, 2140076. <https://doi.org/10.1080/22797254.2022.2140076>

105. Bellotti, P.; Caputo, C.; Davoli, L.; Evangelista, S.; Pugliese, F. Coastal protections in Tyrrhenian Calabria (Italy): Morphological and sedimentological feedback on the vulnerable area of Belvedere Marittimo. *Geogr. Fis. Dim. Quat.* **2009**, *32*, 3–14.

106. D'Alessandro, F.; Tomasicchio, G.R.; Frega, F.; Carbone, M. Design and management aspects of a coastal protection system. A case history in the South of Italy. *J. Coast. Res.* **2011**, *64*, 492–495.

107. Ietto, F.; Cantasano, N.; Pellicone, G. A new coastal erosion risk assessment indicator: Application to the Calabria Tyrrhenian Littoral (southern Italy). *Environ. Process.* **2018**, *5*, 201–223. <https://doi.org/10.1007/s40710-018-0295-6>

108. Cantasano, N.; Pellicone, G.; Ietto, F. The coastal sustainability standard method: A case study in Calabria (southern Italy). *Ocean Coast. Manag.* **2020**, *183*, 104962. <https://doi.org/10.1016/j.ocecoaman.2019.104962>

Disclaimer/Publisher's Note: The statements, opinions and data contained in all publications are solely those of the individual author(s) and contributor(s) and not of MDPI and/or the editor(s). MDPI and/or the editor(s) disclaim responsibility for any injury to people or property resulting from any ideas, methods, instructions or products referred to in the content.